JOURNAL OF GEOPHYSICAL RESEARCH, VOL. 102, NO. C9, PAGES 20,967–20,986, SEPTEMBER 15, 1997

Flow and recirculation of Antarctic Intermediate Water across the Rio Grande Rise

Olaf Boebel,[1] Claudia Schmid, and Walter Zenk
Institut für Meereskunde, Universität Kiel, Kiel, Germany

Abstract. The flow of the low-salinity Antarctic Intermediate Water (AAIW) at 700–1150 m depth across the Rio Grande Rise and the lower Santos Plateau is studied under the auspices of the World Ocean Circulation Experiment (WOCE) in the context of the Deep Basin Experiment. Our data set consists of several hydrographic sections, a collection of 15 RAFOS float trajectories, and records from 14 moored current meters. The data were gathered during different intervals between 1990 and 1994. The inferred flow field strongly supports a basinwide anticyclonic recirculation cell in the subtropical South Atlantic underneath the wind-driven gyre. Its center, which appears to be southeast of the Rio Grande Rise, separates the eastward advection of AAIW below the South Atlantic Current from the westward flowing, recirculating AAIW. The two near-shelf limbs closing the circumference of AAIW flow are formed in the east by the deep Benguela Current, potentially modulated by salty inflow of Indian Ocean Intermediate Water, and in the west by the Brazil Current system. Further important circulation elements are the Brazil-Falkland (Malvinas) Confluence Zone at 40°S and an unnamed divergence at 28°S close to the 1000 m isobath. The resulting broad southward flow of AAIW augments the share of modified, i.e., saltier, intermediate water in the source region of the South Atlantic Current, while the smaller northward flow marks the source of a narrow equatorward Western Intermediate Boundary Current, ultimately leaving the South Atlantic. This shelf-trapped jet is clearly documented in hydrographic data from 19°S and in nearby current meter records. The jet contrasts a sluggish flow across this latitude east of 35°W. A continuous flow of AAIW from its subpolar region in the southwestern Argentine Basin all along the western slope toward the equator appears unlikely between 35°S and 25°S.

1. Introduction

The spreading of Antarctic Intermediate Water (AAIW) in the South Atlantic at about 800 m depth has gained increasing attention during this decade because of its importance in regards to the "great ocean conveyor belt" [*Broecker et al.*, 1985; *Schmitz*, 1995]. The possible pathways of the AAIW at subtropical latitudes in the South Atlantic have been especially subject to a long-standing debate. Since the existence of AAIW in the tropical Atlantic is clearly indicated by a strong salinity minimum and oxygen maximum, an effective transport mechanism from the production site in the South Atlantic northward across the equator must exist. While a direct northward transport is generally accepted north of the Vitória-Trindade Ridge at 20°S, three routes for the advection of the AAIW at midlatitudes between 35°S and 20°S have been discussed: (1) the direct northward flow of AAIW along the western boundary, (2) a northward drift of AAIW with the Brazil Current return flow, and (3) the roundabout transport of AAIW underneath the wind-driven subtropical gyre.

A schematic diagram of the circulation pattern of the intermediate water (Figure 1) in the South Atlantic has been published by *Warner and Weiss* [1992], evaluating large-scale hydrographic parameter and tracer distributions. A subtropical gyre with the South Atlantic Current at its southern boundary is the protruding feature of this diagram between 45°S and 21°S. Originally, *Wüst* [1935], on the basis of his "core layer method," proposed a rather broad direct northward flow of AAIW along the western boundary. This concept was partially supported by *Deacon* [1937] and *Defant* [1941]. *Sverdrup et al.* [1942] estimated the total northward transport of AAIW across 30°S to be 9 Sv (1 Sv = 1×10^6 m^3 s^{-1}). A direct northward advection was also favored by *Evans and Signorini* [1985]. Their study on the spreading of AAIW uses directly measured vertical current and temperature profiles between 24°S and 20°S. Observing northward currents at intermediate depth, they reason that this could support Wüst's concept of a continuous northward western boundary current. However, they note that their measurements do not preclude the westward transport of AAIW south of 24°S and a later deflection to the north at the shelf break, as was proposed about two decades earlier by *Taft* [1963] and *Buscaglia* [1971].

Taft [1963, p. 140] states that "no evidence ... of a continuous northward propagation ..." exists (using *Meteor* 1925–1927 data in the area of interest), whereas *Buscaglia* [1971, p. 253] goes one step further and explicitly excludes a northward current: "it appears that all of the flow south of 37°S is eastward and all of it north of 32°S is westward." In his discussion, Buscaglia gives a comprehensive summary of the relevant publications of the 1950s and 1960s which shall not be repeated

[1]Now at Department of Oceanography, University of Cape Town, Rondebosch, South Africa.

Paper number 97JC00977.
0148-0227/97/97JC-00977$09.00

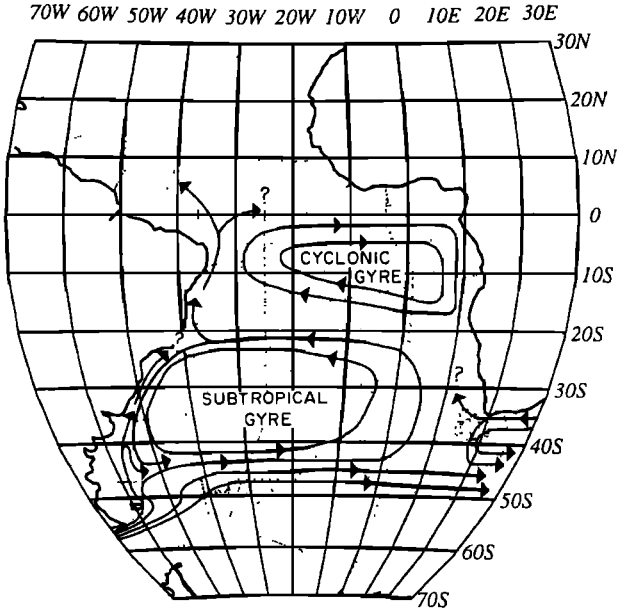

Figure 1. The advection of Antarctic Intermediate Water (AAIW) in the South Atlantic as suggested by *Warner and Weiss* [1992]. Note the question marks at the key points of the AAIW circulation scheme.

here. According to Taft, Buscaglia, and others the northward flowing AAIW at 20°S is derived from AAIW departing eastward from the continental shelf break within the Subtropical Convergence at around 40°S and returning to the Brazilian shelf north of 30°S (Figure 1).

Recent results from a world ocean model by *England and Garçon* [1993] and a South Atlantic model by *Marchesiello* [1995] strongly confirm these considerations. Both indicate an anticyclonic circulation cell of AAIW, resulting in a bifurcation of the northern westward flowing branch at 25°S at the western boundary. The existence of a southward flowing branch, forming the recirculating western segment of the anticyclonic cell, was recently confirmed by *Maamaatuaiahutapu et al.* [1992] in a multitracer study. The latter study derives a southward return flow of AAIW from a systematic southward decrease of the AAIW concentration between 36°S and 39°S, linking the midlatitude tracer distribution to the situation farther south. They suggest that the Subantarctic Surface Water is not the sole source of AAIW but that recirculated AAIW can be a second source, both constituting the eastward flowing limb of the anticyclonic cell.

Some contemporary studies, however [*Suga and Talley*, 1995; *Zemba*, 1991], on the basis of hydrographic data, revived the idea of a direct northward flow to account for an apparent low-salinity tongue extending northward along the shelf at midlatitudes but this time only as a secondary additional path to the dominant flow taking the roundabout route following the wind-driven subtropical gyre. *Zemba* [1991], focusing on the difficulty of finding an adequate reference level for the dynamic method, notes the ambiguousness of velocity fields derived from hydrographic data in this area. In addition to a direct shelf-trapped northward flow, she concludes that a third pathway, underneath the Brazil Return Current, contributes to an effective northward transport of AAIW.

Reid [1989], giving probably the most comprehensive study of the South Atlantic's general circulation, discussed both the idea of a continuous equatorward flow of AAIW along the western boundary as well as the concept of an anticyclonic basinwide loop underneath the subtropical gyre. *Reid* [1989, p. 187] concludes that both possibilities are consistent with the data available and that direct measurements are needed to resolve this important question: "The presence of a narrow northward flow from 35°S to 25°S in the far west at the depth of the salinity minimum is not demonstrated by the present data set, nor is it entirely precluded. Perhaps direct measurements near 30°S would be required to resolve the matter."

Whereas *Reid*'s [1989] nonsynoptic study was performed on an oceanwide scale, our study focuses on the possible westward flow of AAIW around 30°S between 25°W and the Brazilian shelf. Motivated by Reid's concluding remarks and by the objective of the World Ocean Circulation Experiment (WOCE) drifter program [*World Climate Research Program (WCRP)*, 1988] to obtain a reference level for geostrophic calculations by means of deep Lagrangian drifters, an attempt is made to combine information from direct measurements of the distribution of hydrographic properties and direct current measurements (Lagrangian or Eulerian). This two-pronged approach should give a comprehensive picture of the general circulation at intermediate depths west of the Rio Grande Rise (Figure 2).

Section 2 gives an overview of the working area and the conducted measurements along with their methodical limitations. This section, as well as the subsequent ones, generally deals first with hydrographic data and then with the RAFOS float data followed by data from the moored current meters. Section 3 gives a description of our observational results, which are sections of salinity, potential temperature, and potential density, together with float trajectories and stick plots inferred from current meter data. Section 4 deals with properties derived from this data base, for example, geostrophic calculations derived from the hydrographic sections, statistical analysis of the float and current meter data, and energetic calculations. Section 4 closes with a comparison of transport calculations based on the three different data sources. Section 5 casts these results in a coherent concept under consideration of the available literature.

2. Experiments and Methods

The hydrographic data used herein consist of two zonal WOCE Hydrographic Program (WHP) sections (A9 and A10) across the subtropical South Atlantic. The locations of the western part of these sections are shown as small dots in Figure 2. The northern section A9 at 19°S was occupied by *Meteor* (cruise 15, leg 3) from February to March 1991 [*Siedler and Zenk*, 1992]. The southern transect A10 at 30°S was taken from December 1992 through January 1993 (*Meteor* cruise 22, leg 5) [*Siedler et al.*, 1993]. Additional shorter sections spanning the region of the Brazil Current were obtained during legs 1 and 2 of *Meteor* cruise 15 between December 1990 and January 1991 and *Meteor* cruise 22, legs 3 and 4, in December 1992. The station spacing of the two WHP sections varies between 10 to 30 nautical miles (19 and 56 km) near the shelf and 50 to 60 nautical miles (93 and 111 km) in the interior ocean. The Brazil Current sections cover the continental slope from 200 m to more than 3000 m depth with a station spacing of up to 60 nautical miles (111 km). The conductivity-temperature-depth (CTD) data quality conforms to WOCE standards [*WCRP*, 1994].

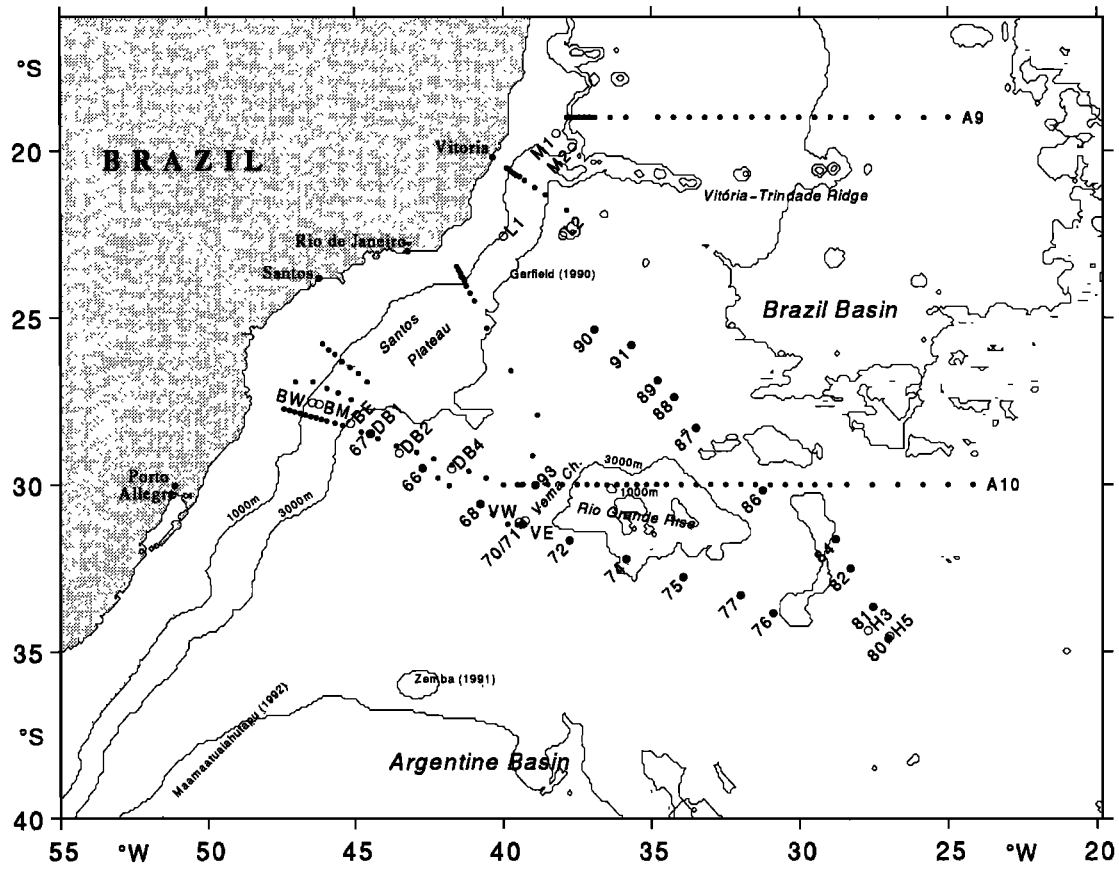

Figure 2. Topography of the subtropical western South Atlantic with isobaths at 1000 and 3000 m indicated by thin solid lines. Small dots mark the positions of two World Ocean Circulation Experiment (WOCE) hydrographic sections taken during *Meteor* cruises 15 and 22 and of four additional sections spanning the Brazil Current. Solid circles paired with two digits indicate launch positions of RAFOS floats during *Meteor* cruise 22. Open circles indicate the positions of moorings, each labeled with its respective identifier (Table 2). Boxes (thin dotted lines) indicate the areas studied by *Maamaatuaiahutapu et al.* [1992], *Zemba* [1991], and *Garfield* [1990].

During *Meteor* cruise 22, legs 4 and 5, 21 RAFOS floats were deployed in the subtropical South Atlantic around the Rio Grande Rise to obtain Lagrangian current observations. All instruments were built and preballasted at the Institut für Meereskunde in Kiel (IfM Kiel) [*König and Zenk*, 1992]. Since the main objective of this cruise was to recover and deploy current meter moorings in the Vema and the Hunter Channels, the deployment sites of four sound sources, indispensable for the acoustic tracking of RAFOS floats, and float launch positions were constrained by logistic necessities. Equidistant float launch sites along the cruise track were chosen, resulting in an interfloat spacing of ~100 km (Figure 2, solid circles 66 through 93). All floats were launched within 16 days from December 4, 1992, to December 19, 1992 (Table 1), except for one float (float 93) which was launched on January 4, 1993, during *Meteor* cruise 22, leg 5. The float weights were adjusted individually to reach neutral buoyancy around 900 m depth, close to the salinity minimum of the AAIW. The instruments recorded pressure, temperature, and sound signal travel times for three listening windows once a day.

Because of leaks in both the hydrophone feedthrough as well as the release plug, six floats surfaced prematurely within a week or so. Trajectories of the remaining 15 floats were obtained, resulting in 6.2 float years of data. From these 15 floats, 10 floats (floats 67, 70, 71, 72, 74, 86, 87, 88, 89, and 91) suffered from small leaks which made them sink slowly: One float (float 71) sunk to the emergency pressure release level of 1350 dbar and, consequently, surfaced prematurely after 45 days, whereas the other nine showed self-sealing at greater depths, resulting in underwater drifts covering a pressure range from 738 dbar up to 1355 dbar. Some of the slowly sinking floats did receive the sound sources only weakly (float 67, days 100–200; float 74, days 50–200; float 86, days 80–130; and float 91, days 1–70), most likely because of the technical problems described above. These gaps in the time of arrival data were interpolated linearly. The remaining five floats (floats 66, 76, 84, 90, and 93) recorded only small pressure fluctuations of the order of 50 dbar and, consequently, are considered to be tight. The start and end points of the trajectories were traceable within 5 km of the launch and first surface position of the float. Some floats had to be tracked across the connecting line between two sound sources (baseline crossing). This results in a reduced local accuracy or unsteady behavior of the position data. However, in a statistical sense these jumps are compensated if a larger data segment around the baseline crossing is considered.

The Eulerian velocity data set comprises a chain of current meters (open circles in Figure 2, labeled BW, BM, BE, DB1,

Table 1. Float Mission Parameters and Averages

Float	Launch Position	Launch Date	Mission Length, days	Pressure Range, dbar	$\overline{\lvert v \rvert}$, cm s^{-1}	mke, J m^{-3}	eke, J m^{-3}	Heading, °T
66	29°31'S, 42°42'W	Dec. 4, 1992	90	767–808	6.5	2.1	0.6	239
67	28°27'S, 44°27'W	Dec. 3, 1992	270	828–1259	2.4	0.3	3.9	215
70	31°12'S, 39°02'W	Dec. 8, 1992	180	826–1314	3.1	0.5	0.9	258
71	31°12'S, 39°21'W	Dec. 8, 1992	47	779–1347	4.5	1.0	0.8	304
72	31°40'S, 37°45'W	Dec. 9, 1992	90	898–1115	5.7	1.6	0.6	276
74	32°14'S, 35°50'W	Dec. 9, 1992	324	813–951	3.0	0.5	1.2	281
76	33°51'S, 30°53'W	Dec. 11, 1992	90	911–955	2.6	0.3	0.2	203
84	31°38'S, 28°47'W	Dec. 16, 1992	90	992–1034	5.2	1.4	0.2	288
86	30°11'S, 31°15'W	Dec. 17, 1994	331	824–941	3.2	0.5	1.4	258
87	28°18'S, 33°30'W	Dec. 18, 1992	90	794–1355	3.4	0.6	0.4	298
88	27°23'S, 34°14'W	Dec. 18, 1994	29	839–977	2.1	0.2	0.1	0
89	26°53'S, 34°47'W	Dec. 19, 1994	90	786–849	0.7	0.2	0.2	7
90	25°22'S, 36°55'W	Dec. 19, 1992	180	738–794	2.3	0.3	0.7	298
91	25°50'S, 35°40'W	Dec. 19, 1992	360	847–1248	1.8	0.2	0.6	262
93	30°01'S, 38°55'W	Jan. 1, 1993	139	802–827	5.1	0.8	1.3	264

All floats but 93 were launched within a few days after their start date. Float 93 was launched January 4, 1993. The mean float speed ($\overline{\lvert v \rvert}$), the mean and eddy kinetic energy density (mke and eke), and the direction of each float's total displacement (heading) are given.

DB2, DB4, VW, and VE), representing a mooring array across the Santos Plateau from the Brazilian shelf to the Rio Grande Rise. Moorings were jointly provided by the IfM Kiel and the Woods Hole Oceanographic Institution (WHOI). Deployments were accomplished during *Meteor* cruise 15 in austral summer 1990/1991 [*Siedler and Zenk*, 1992]. In the course of *Meteor* cruise 22 these current meters were recovered (Table 2). A second set of moorings (H3 and H6) was deployed in the Hunter Channel during the same cruise. The latter were recovered in May 1994 (*Meteor* cruise 28 [*Zenk and Müller*, 1995]). Data of two additional current meters on the shelf edge at 22°S (JL1 and JL2) were kindly provided by J. Lima (personal communication, 1992). They were deployed for intermittent periods during August 1991 through March 1992. Mean values of the two current meter records just north of the Vitória-Trindade Ridge (TM1 and TM2) were provided by *Müller et al.* [1994]. They represent data from November 1989 through March 1990. From the nine IfM Kiel/WHOI current meters at the AAIW level west of the Rio Grande Rise at the AAIW level, eight instruments produced data [*Tarbell et al.*, 1994]. Exact positions, record lengths, and calculated means of all instruments mentioned are given in Table 2.

3. Observational Results

Sections of salinity S, potential temperature θ, and potential density, referenced to 1000 (σ_1) and 3000 dbar (σ_3), of the western part of the two WHP transects are presented in Figures 3 and 4. Both sections clearly exhibit the salinity minimum of the AAIW, located below the thermocline at 800–1000 m depth. Using *Peterson*'s [1992] definition of the AAIW layer as being framed by potential density surfaces $\sigma_1 = 31.53$ kg m^{-3} and $\sigma_1 = 31.98$ kg m^{-3}, a vertical extension of about 500 m is observed. The core depth itself is rising from 900 dbar at 30°S to about 800 dbar at 19°S in between the two sections. The core salinity increases from the southern to the northern section by nearly 0.1 from less than 34.30 to values around 34.40. This increase is associated with an increase of the potential temperature (from 4.0°C to 4.5°C), resulting in an increase of the

Table 2. Eulerian Statistics of Current Meter Records

Mooring	Position	Depth, dbar	Number of Data Points, days	T, °C	$\overline{\lvert v \rvert}$, cm s^{-1}	Heading, °T	T_{uu}, days	T_{vv}, days
BW	27°54'S, 46°43'W	875	681	4.57	2.0 ± 0.4	296	3	8
BM	27°59'S, 46°21'W	930	681	4.47	3.7 ± 0.4	218	5	8
BE	28°16'S, 45°14'W	950	680	4.31	1.5 ± 0.7	252	24	8
DB1	28°28'S, 44°28'W	908	696	4.42	4.2 ± 0.7	278	14	24
DB2	29°03'S, 43°30'W	895	96	4.46	7.0 ± 1.9	249	10	12
DB4	30°05'S, 41°44'W	914	694	4.47	2.2 ± 0.5	255	13	17
VW	31°12'S, 39°46'W	840	683	5.02	1.6 ± 0.7	257	28	21
VE	31°08'S, 39°26'W	900	682	3.98	1.5 ± 0.7	267	27	19
H3	34°22'S, 27°42'W	905	520	3.94	0.9 ± 0.7	307	24	16
H6	34°32'S, 26°59'W	890	518	3.96	0.3 ± 0.4	92	20	9
L1	22°33'S, 40°01'W	927	63	3.74	19.4 ± 1.1	40	...	...
L2	22°33'S, 38°00'W	948	53	3.66	2.3 ± 1.7	260	...	...
M1	38°12'S, 19°29'W	750	...	...	20.8	64	...	...
M2	37°39'S, 19°53'W	750	...	...	6.1	309	...	...

For the locations, see Figure 2. The mean temperature T, the mean speed $\overline{\lvert v \rvert}$, and the mean direction (heading) of the flow are given. The integral timescales T_{uu} and T_{vv} indicate the integral of the autocorrelation function at time lag 100 for zonal and meridional velocity components, respectively.

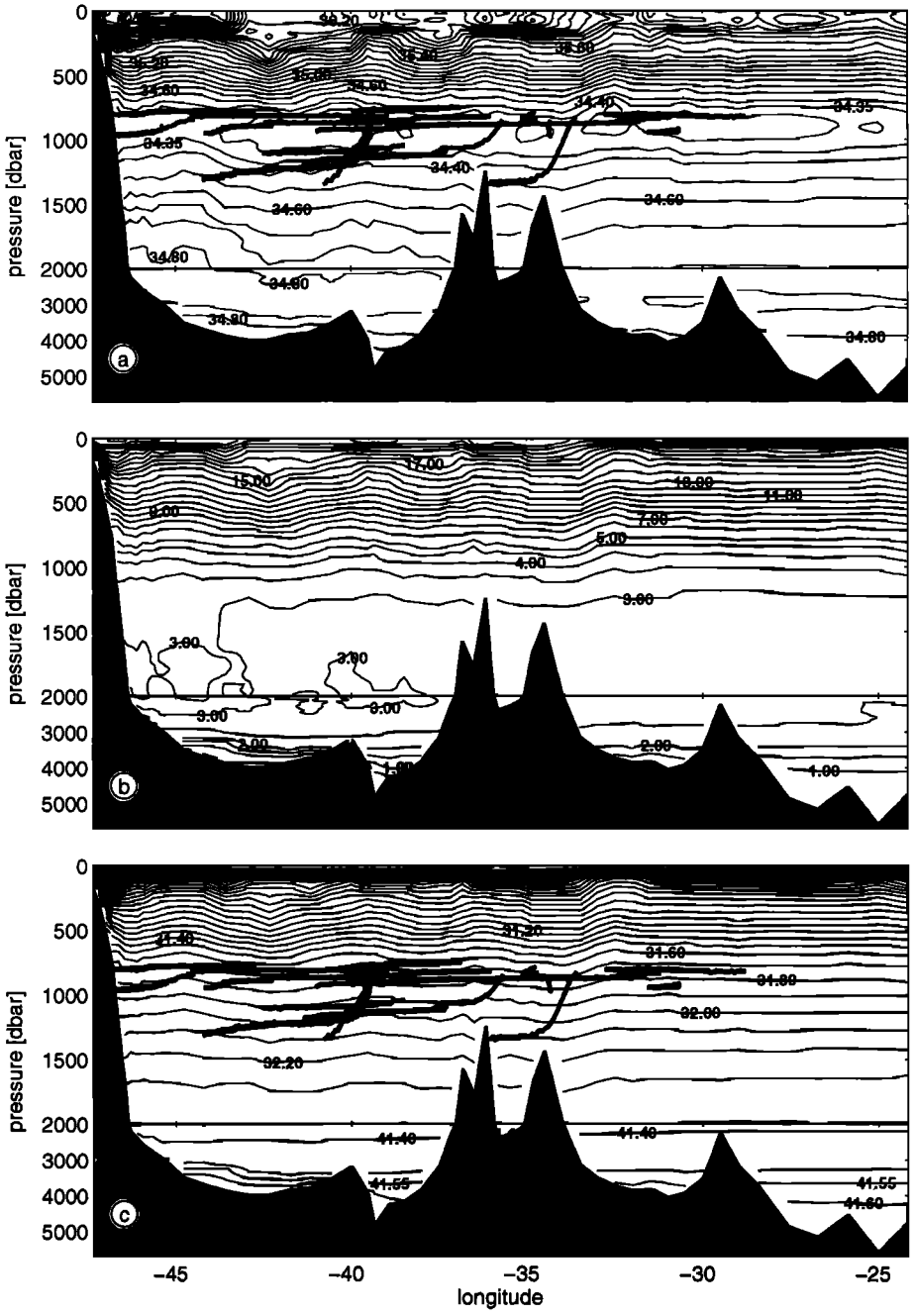

Figure 3. Hydrographic section at 30°S (WOCE section A10, *Meteor* cruise 22, leg 5, taken from December 28, 1992, to January 28, 1993), western part only: (a) salinity, (b) potential temperature, and (c) density (σ_1 isolines in the upper 2000 dbar and σ_3 isolines below 2000 m). The contour interval of the isohalines equals $\Delta S = 0.1$, with an additional isoline at $S = 34.35$ to mark the salinity minimum more clearly. Isotherms are spaced by 1.0°C for $\theta > 5$°C and by 0.5°C for $\theta < 5$°C. Contour intervals of σ equal 0.1 kg m^{-3}. Thick solid lines in Figures 3a and 3c indicate trajectories of RAFOS floats projected on the section.

core's potential density anomaly σ_1 from 31.80 kg m^{-3} at 30°S to 31.86 kg m^{-3} at 19°S (Figures 3c and 4c).

A lateral salinity minimum core is not observed at the western shelf break within the low-salinity AAIW layer in the 30°S section. In contrast, the 19°S section exhibits such a lateral core, featuring a minimum with salinities <34.35 at the western boundary. Additional shorter sections (see Figure 2 for positions) spanning the Brazil Current at nominal 21°S [*Schmid et al.*, 1995], 24°S (Figures 5b and 5c), and others (not shown) confirm this meridional dependency. Only sections north of 21°S (Figures 5a and 5b) show a lateral salinity minimum in the west ($S < 34.35$), whereas no such extremum is observed in the sections south of 24°S (Figures 5c and 5d), which exhibit a homogenous salinity minimum of $S > 34.35$ throughout the AAIW layer.

The lateral minimum salinity distributions (Figure 6) on both WHP sections show a common west to east gradient of the AAIW core salinity, though considerable differences exist

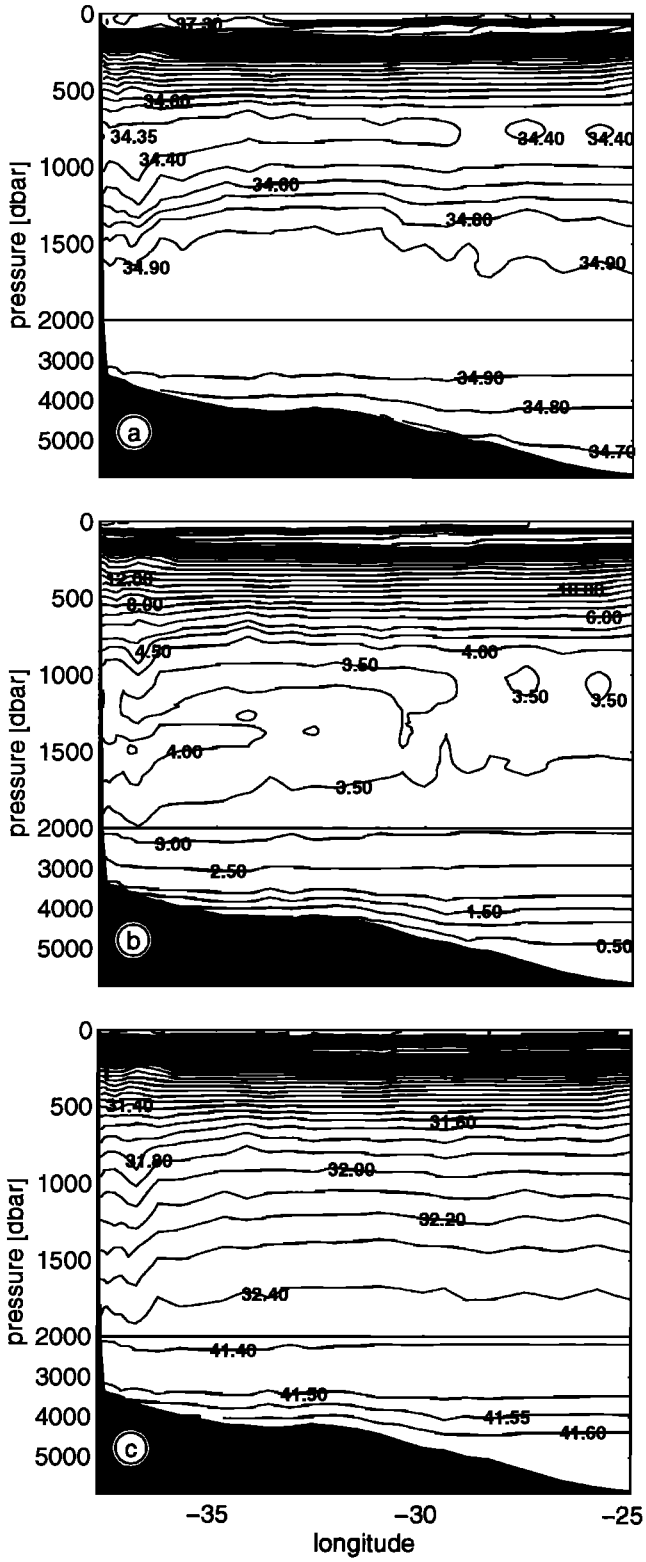

Figure 4. Hydrographic section at 19°S (WOCE Hydrographic Program (WHP) section A9, *Meteor* cruise 15, leg 3, taken from February 11 to March 20, 1991), western part only: (a) salinity, (b) potential temperature, and (c) density (σ_1 isolines in the upper 2000 dbar and σ_3 isolines below 2000 m). The contour interval of the isohalines equals $\Delta S = 0.1$, with an additional isoline at $S = 34.35$ to mark the salinity minimum more clearly. Isotherms are spaced by 1.0°C for $\theta > 5$°C and by 0.5°C for $\theta < 5$°C. Contour intervals of σ equal 0.1 kg m^{-3}.

in details. The zonal salinity increase in the AAIW core layer at 30°S is smaller than at 19°S, whereas a larger variability of the local core salinity is observed in the south. Here, at 30°S we note fairly regular fluctuations (Figure 6 and Table 3) of the core salinity, superimposed on a moderate trend (0.001 deg^{-1}). In contrast, the minimum salinity distribution at 19°S exhibits smaller modulations but a stronger gradient. At 30°S the sa-

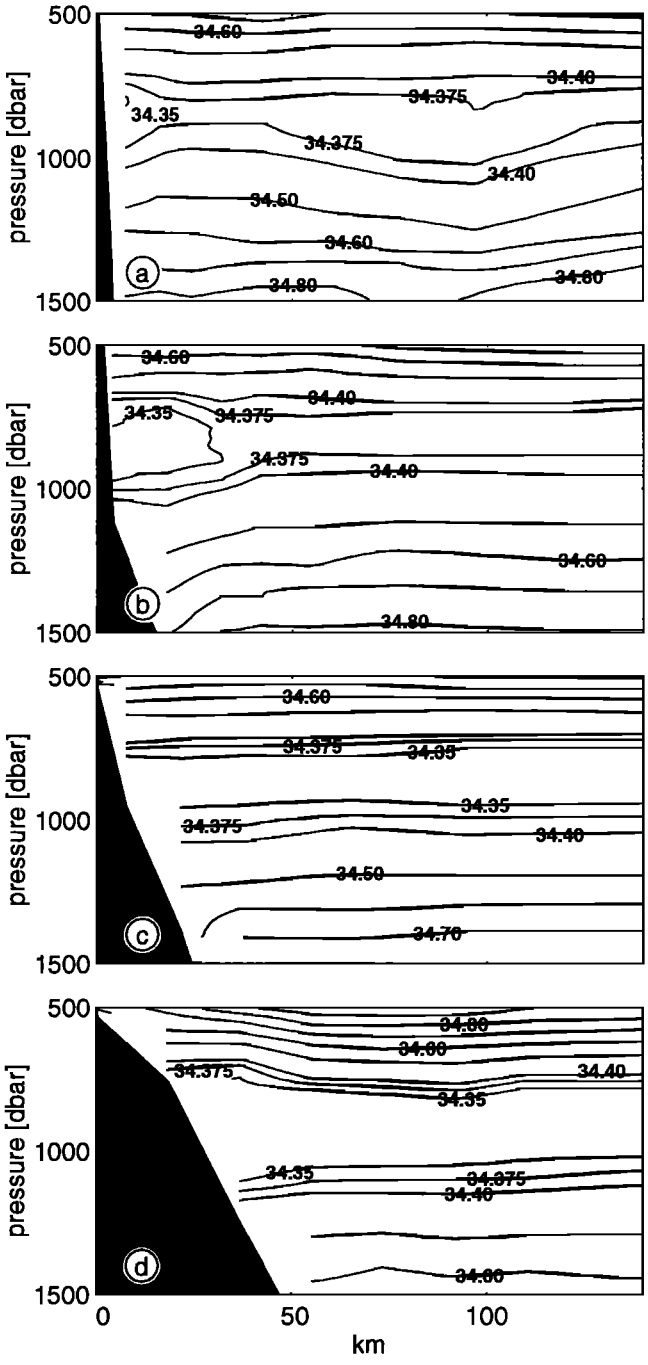

Figure 5. Salinity sections across the Brazil Current (a) near 19°S, (b) near 21°S, (c) near 24°S, and (d) near 28°S. The section at 28°S is the westernmost part of the 30°S WHP A10 section, which had a course perpendicular to the bottom slope at the western shelf break. For exact positions, see Figure 2. Note the isoline ($S = 34.375$) in addition to those shown in Figures 3 and 4. Otherwise, the contour interval of the isohalines equals $\Delta S = 0.1$.

linity distribution shows three distinct salinity minima around 40°W, around 29°W, and at 18°W. The amplitude of these deviations is increasing from the west ($\Delta S = 0.04$) to the east ($\Delta S = 0.06$). The interpatch distance amounts to about 1170 km.

In addition to the isolines, Figures 3a and 3c contain our float trajectories projected onto the 30°S CTD section which was occupied about 1 month after the float deployments. Most floats stayed within the AAIW depth horizon, defined by the region with salinities $S < 34.4$ (this value corresponds approximately to the density limits of the AAIW layer mentioned above). Floats 67, 70, 71, 87, and 91 sank only slightly (up to 200 m) below the defined lower limit of the AAIW at approximately 1150 dbar. Hence the dynamic behavior of the AAIW appears to be fairly well represented by the floats of this experiment.

Trajectories of all floats are plotted in Figure 7. The launch sites are indicated by dots with the corresponding float number to the right. A general westward drift of these instruments is clearly visible. Whereas the southern instruments follow a direct westward course, the northern group drifts in a northwestern direction before being deflected to the southwest while approaching the shelf break. Individual mean speeds (Table 1) range from 0.7 to 6.5 cm s^{-1}, mean kinetic energy densities (mke) cover a range from 0.2 to 2.1 J m^{-3}, similar to the range of eddy kinetic energy densities (eke) (0.1–3.9 J m^{-3}).

Pressure, temperature, and velocity data of floats 66 and 84, representative of all five floats classified as "tight" in section 2, are displayed in Figure 8. Float 66 shows an increase in pressure by 25 dbar from 775 to 800 dbar between days 45 and 55, correlated with an increase in temperature by 0.4°C from 5.7°C to 6.1°C. During the same period the meridional velocity component v indicates a southward extremum of 8 cm s^{-1}. Float 84 measured a decrease in pressure over 20 dbar from 825 to 805 dbar between days 30 and 55. The observed pressure change is linked to a decrease in temperature from 5.2°C to 4.8°C and a slightly increased northward velocity component. The linkage between the pressure and temperature records of floats 66 and 84 indicates that this motion might be due to the sinking or shoaling of the water layer enveloping the float [*Rossby*, 1988].

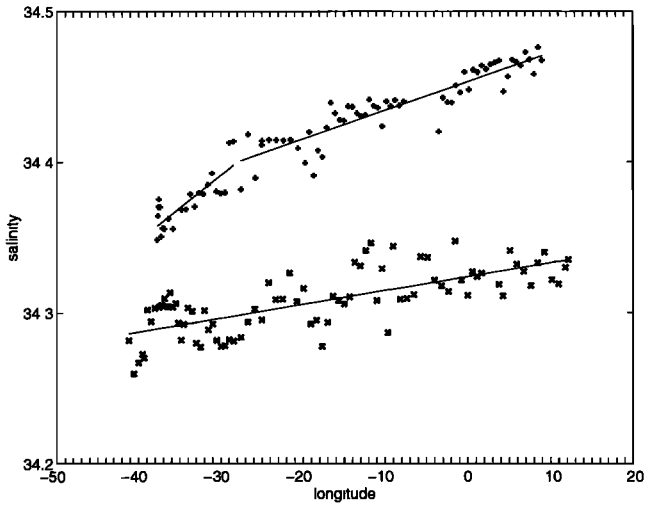

Figure 6. Longitude dependence of the salinity minimum in the AAIW core at 19°S (top curve) and near 30°S (bottom curve). The data were restricted to a corridor of ±0.1° around the nominal latitude and to a depth of between 600 and 1200 dbar. Linear fits are applied at 19°S, one covering the region between 37.59°W and 28.44°W and the other covering the region between 27.45°W and 8.08°E. At 30°S a single linear fit is applied for the whole part of the section shown herein. The fit parameters are given in Table 3.

Table 3. Fit Parameters for the Salinity Trend in the Core Layer of the Antarctic Intermediate Water

	Slope, deg^{-1}
19°S, western part	4.3×10^{-3}
19°S, eastern part	1.9×10^{-3}
30°S	0.9×10^{-3}

Compare with Figure 6.

Using the pressure and temperature data of floats 66, 76, 84, and 93, an effort has been made to calculate the salinity of the surrounding water [*Boebel et al.*, 1995] using the assumption of density equilibrium between the float and the surrounding water. As shown in Figure 9, the TS diagrams of floats 66 and 84 match their associated TS diagrams, taken prior to the launch with the CTD. This indicates that these floats stayed with their corresponding water body for their entire mission length and that the properties of the surrounding waters did not change during that period. Similar results were obtained for the other two floats (not shown). This perception implies that our RAFOS floats observe little mixing along their way, in agreement with *von Schubert*'s [1935] and, more recently, *Reid et al.*'s [1977] observation that the stability of the water column increases at layer interfaces, especially above the AAIW at ~500 m, as well as below, resulting in a reduced mixing rate across these interfaces. It also hints at a predominantly advective spreading within the observed westward current band.

It is remarkable that the simple, fundamental process of vertical displacement of a water parcel seems to be responsible for the fluctuations observed in the pressure and temperature data collected by these floats and that the fluctuations are frequently correlated with increased zonal or meridional speeds of the floats (floats 66 and 76). The changes in pressure and temperature occur mostly on the rather short timescales of 20 days (sinking of float 66), being framed by periods of invariant stratification and thus stable pressure records.

Figure 10 depicts vector diagrams of data from several moored current meters (see Figure 2) representative of different regimes within the AAIW. The data presented are described by *Tarbell et al.* [1994]. In Figure 10a the westernmost current meter (Brazil Current West, BW) close to the Brazilian shelf, 305 m above the seafloor at 875 m depth, is shown. A bidirectional structure of the current at the AAIW level is observed. On timescales of ~2 weeks the current alternates between northward and southward directions resulting in a double-peaked flow distribution with meridional means of 9.2 cm s^{-1} to the north and 7.8 cm s^{-1} to the south. The preferred flow directions are not exactly antiparallel (345°T versus 188°T) as should be expected by a complete topographical control, which is the result of a stable zonal velocity component.

Figure 10b depicts data from a current meter (Brazil Current Middle, BM) moored at the upper Santos Plateau. The flow is predominately to the south, with occasional undulations in mainly westward directions. Like the neighboring current meter BW, it recorded a strong current event during the first 100 days. Thereafter, however, the two records appear to be

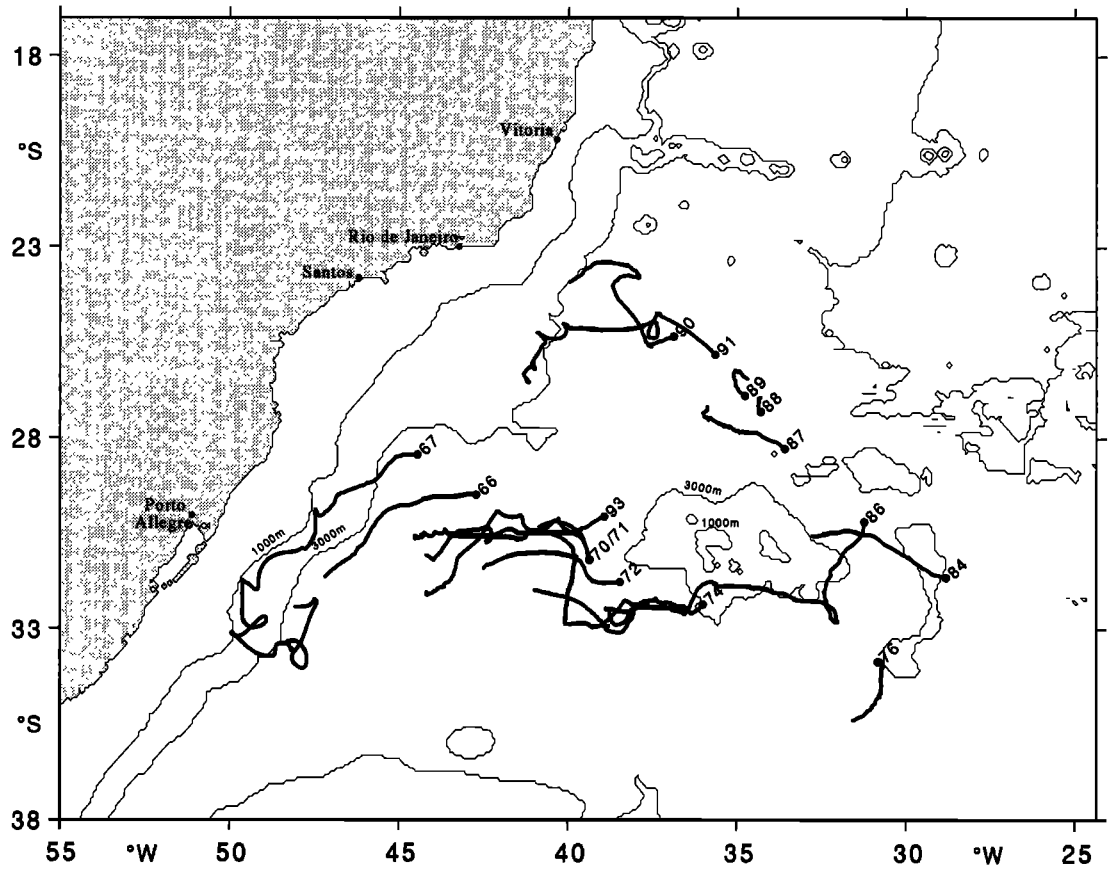

Figure 7. Trajectories of RAFOS floats (thick curves) launched during *Meteor* cruise 22, with dots and neighboring float numbers indicating their launch positions. Please note that the trajectories represent float drifts of varying mission lengths (1–12 months).

minimally correlated. The situation at the lower Santos Plateau around 908 m depth is represented by the current meter (Deep Basin 1, DB1) depicted in Figure 10c. Here a rather constant westward flow is observed (please note the rotation of the reference arrow), whereas eastward excursions rarely happen. Finally, Figure 10d presents data from a current meter in the Vema Channel (Vema Channel West, VW). It depicts a small undulating flow, however, with a preference toward westward directions.

4. Analysis

This section presents the velocity distributions derived from the various data sets. First, using the dynamic method, geostrophic velocities are calculated from the hydrographic data. A statistical analysis of the float data with a subsequent examination of the current meter data with respect to temporal variability and the stability of the long-term means follows. The section closes with a comparison of transports obtained from the various data sets.

Figures 11 and 12 show the geostrophic velocities at 30°S and 19°S, respectively, relative to the depth of the $\sigma_3 = 41.55$ kg m^{-3} isopycnal density anomaly. This level is located between the North Atlantic Deep Water (NADW [*Wüst*, 1935]) and the Weddell Sea Deep Water (WSDW [*Reid et al.*, 1977]). *Stramma and Peterson* [1990] and *Suga and Talley* [1995] used similar reference levels for their studies on the basin-scale circulation. In addition, this choice results in a velocity distribution consistent with the velocity field derived from the IfM Kiel/WHOI current meter array [*Tarbell et al.*, 1994], as will be seen below.

At 30°S the geostrophic velocities (Figure 11) within the AAIW layer west of 42°W are mainly southward, with the strongest current near the shelf break. East of 32°W the currents are weaker and more variable. The observed low-salinity patches around 40°W, 29°W, and 18°W (see section 3 and Figure 3) at the AAIW level are uncorrelated with the calculated geostrophic velocity field. Farther north at 19°S, equatorward velocities are dominant at the AAIW horizon, especially in the western half of this section (Figure 12). The northward western boundary current expected at this latitude appears to be masked by an eddy-like structure near 37°W, which consists of two velocity cores with nearly the same speeds but opposite signs. Its velocity maximum is located at about 600 dbar. Maximum northward (southward) speeds in the AAIW level are restricted to the eddy-like structure, amounting to 35 and -30 cm s^{-1}, respectively. To the west of this structure, below the southward Brazil Current, a narrow northward jet of 25 cm s^{-1} exists, which is coincident with the local salinity minimum observed there (see section 3 and Figure 5a).

The following analysis of the float data will be presented in statistical terms. In total, 2251 velocity values were obtained, which equals 6.2 float years of data. This means that a data density of ~25% of the desired WOCE goal [*WCRP*, 1988] of

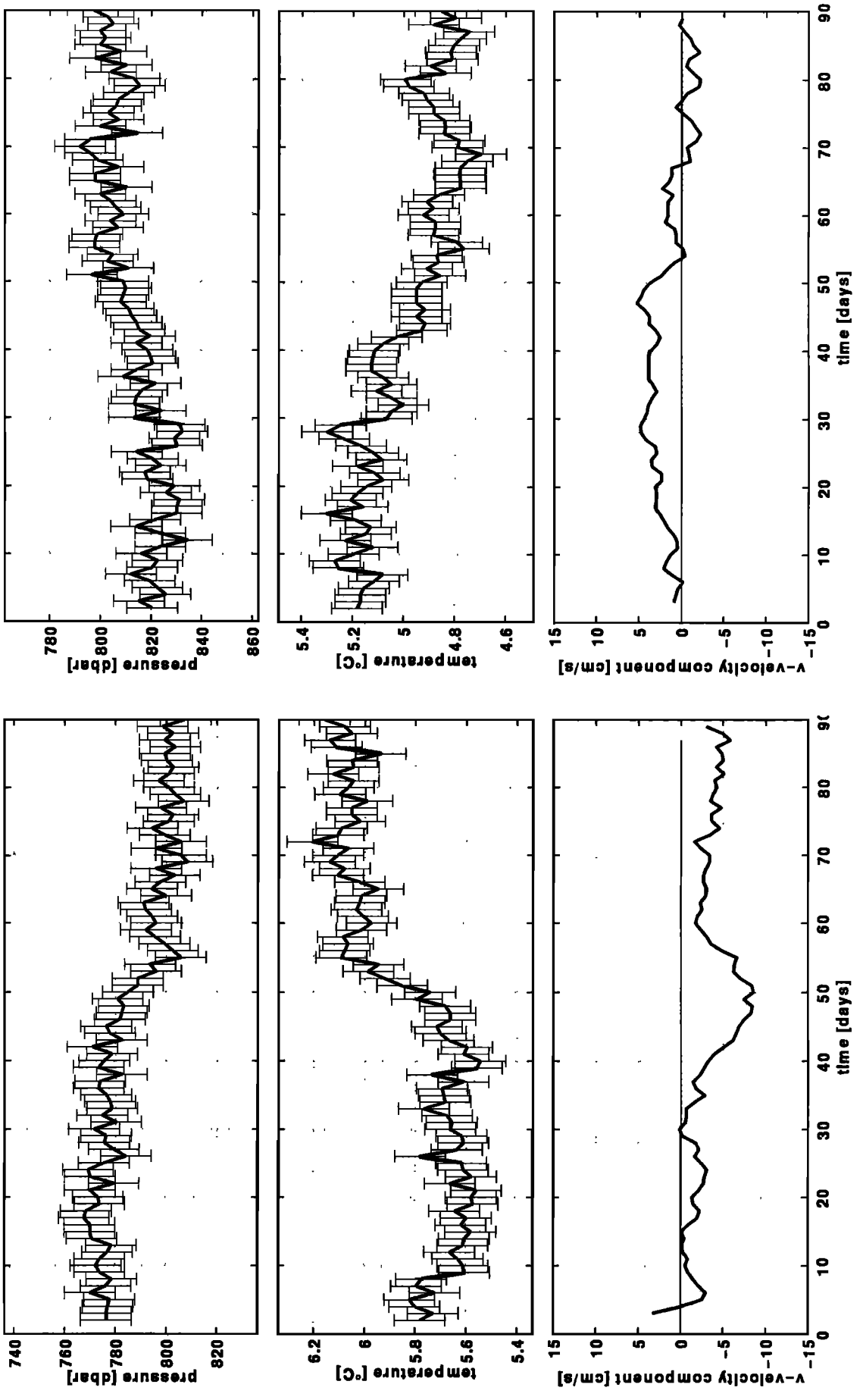

Figure 8. Pressure, temperature, and meridional velocity data for floats (left) 66 and (right) 84.

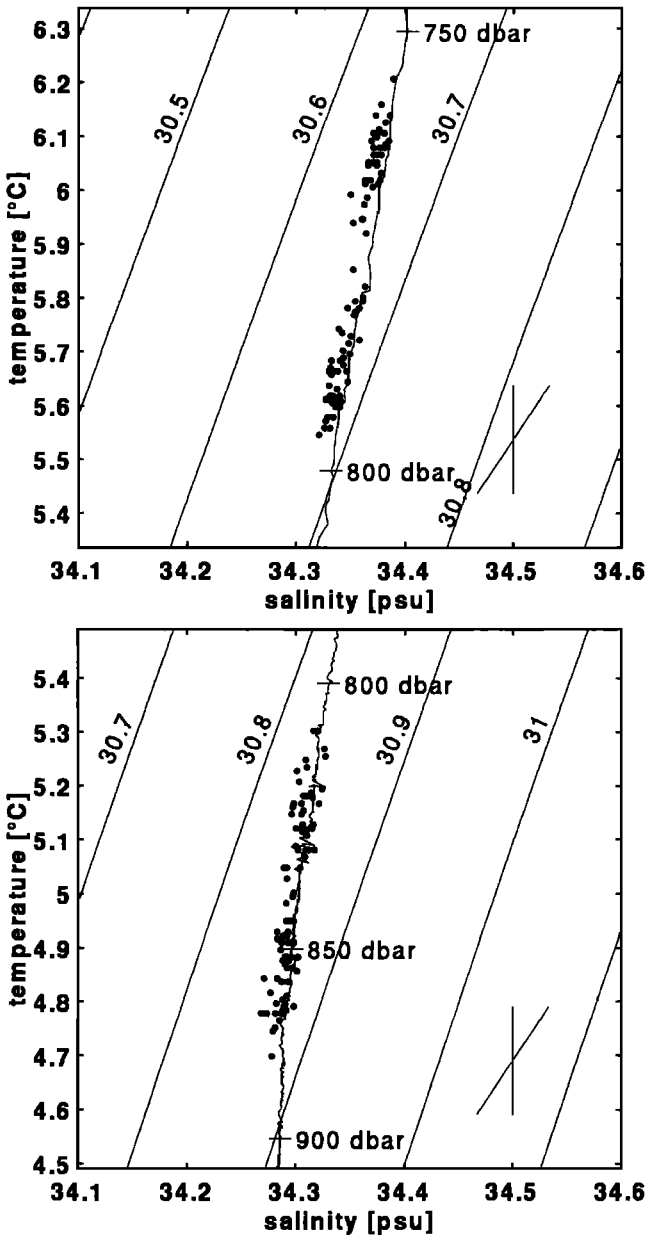

Figure 9. TS diagrams of floats (top) 66 and (bottom) 84. Dots represent temperature and derived salinity data based on daily float pressure and temperature measurements. The solid curve indicates the TS diagram obtained by a CTD cast prior to the float launch. Additional solid lines indicate isopycnals σ referenced to the mean float depth and labeled in units of $[\sigma] = \text{kg m}^{-3}$. Note the error bars in the bottom right corner.

5 float years per 5° by 5° box was achieved for the area covered. For each float the daily velocity data are calculated as the centered difference of the position data over a 2-day cycle. In the following calculations the unfiltered data set is used.

To obtain a planar, spatially resolved description of the mean circulation, a transition from the Lagrangian to the Eulerian frame is rendered. This transition provides a representation of the float velocities independent of variable mission lengths. It further makes the float data comparable to other measurements which are usually obtained and presented in the Eulerian framework. The float data are presented in terms of vector fields representing the mean velocity and error estimates thereof as well as scalar fields describing mean and eddy kinetic energy. To maintain the highest data density possible, all 15 trajectories are used to calculate the statistical properties presented below, regardless of float depth or data interpolations. Thus the properties described in the following should be considered as a rough estimate representative of the physics of the AAIW layer or, more precisely, a water layer between 800 and 1350 dbar. The analysis is cast into a 2° by 2° grid. The number of data points, regardless of float depth or residence time, and the number of corresponding floats are given in Figure 13 for each box. Data are displayed only if the corresponding box contains at least 30 valid points. Because of the daily sampling rate of the floats, this corresponds to a data density of at least 30 float days. The overall data density is still low for statistical purposes, but it appears to be fortuitous that the float motion was surprisingly smooth and uniform.

The resulting velocities are presented as solid arrows in Figure 14. In addition to the westward drift already observed in the float trajectories (Figure 7) the strength of the westward drift is revealed to be of the order of 3 cm s^{-1}. Close to the shelf break, a southwestward drift parallel to the isobaths of the continental slope with undiminished strength is indicated. The northern part of the westward flowing AAIW first moves slowly to the northwest before being deflected to the southwest. In the vicinity of the Vema Channel the flow seems to deviate northward from a straight westward motion, which is resumed farther west.

The significance of the means is presented in terms of the 63% probability error ellipses ε_{ij} calculated for every 2° by 2° box (Figure 14) after a principal axis frame transformation was rendered. The error of each velocity component was calculated according to $\varepsilon_{ij} = \pm q_{0.815} s_{ij} / \sqrt{N'_{df}}$. Here $q_{0.815}$ is the 0.815 percentile of the Student's t-distribution, and s_{ij} equals the variance of the velocity vector for each box with respect to the corresponding box velocity mean. The effective number of degrees of freedom N'_{df} was chosen to be the larger value of either N_{df}, described below, or the number of floats occupying the specific box. The number of degrees of freedom N_{df} is given by $N_{\text{df}} = (1/2T) N \Delta t$, where N is the number of data points per box (Figure 13), Δt is the measurement period (1 day for these floats), and T is the Lagrangian integral timescale. For T we chose 16 days, a value which is observed for both the zonal ($\overline{T_{uu}}$ = 16.2 days) and meridional ($\overline{T_{vv}}$ = 15.4 days) ensemble-averaged integrated zonal velocity autocorrelation functions at time lag 100 [*Ollitrault*, 1994] and which is supported further by the Eulerian observations (see below). It is about 3 times the value used in North Atlantic float studies (T = 5 days) [*Richardson*, 1991], thus being a conservative assumption paying respect to the smoothness of our float trajectories. From Figure 14 it is evident that all but the means close to the shelf break differ significantly from zero. The large error ellipses at the continental slope are mainly due to the high eddy activity captured by float 67 (Figure 7).

The map of eddy kinetic energy density (open circles in Figure 15), in comparison with mean kinetic energy density (solid circles), depicts a regional dependence. For most of the boxes in the open ocean the mean kinetic energy is somewhat larger than the eddy kinetic energy, but the southern boxes at the western boundary exhibit a large dominance by the eddy kinetic energy. The spatial distribution of the mean kinetic energy is particularly uniform along a zonal band covering 31°S–29°S.

Similar calculations can be made for the last data type, the

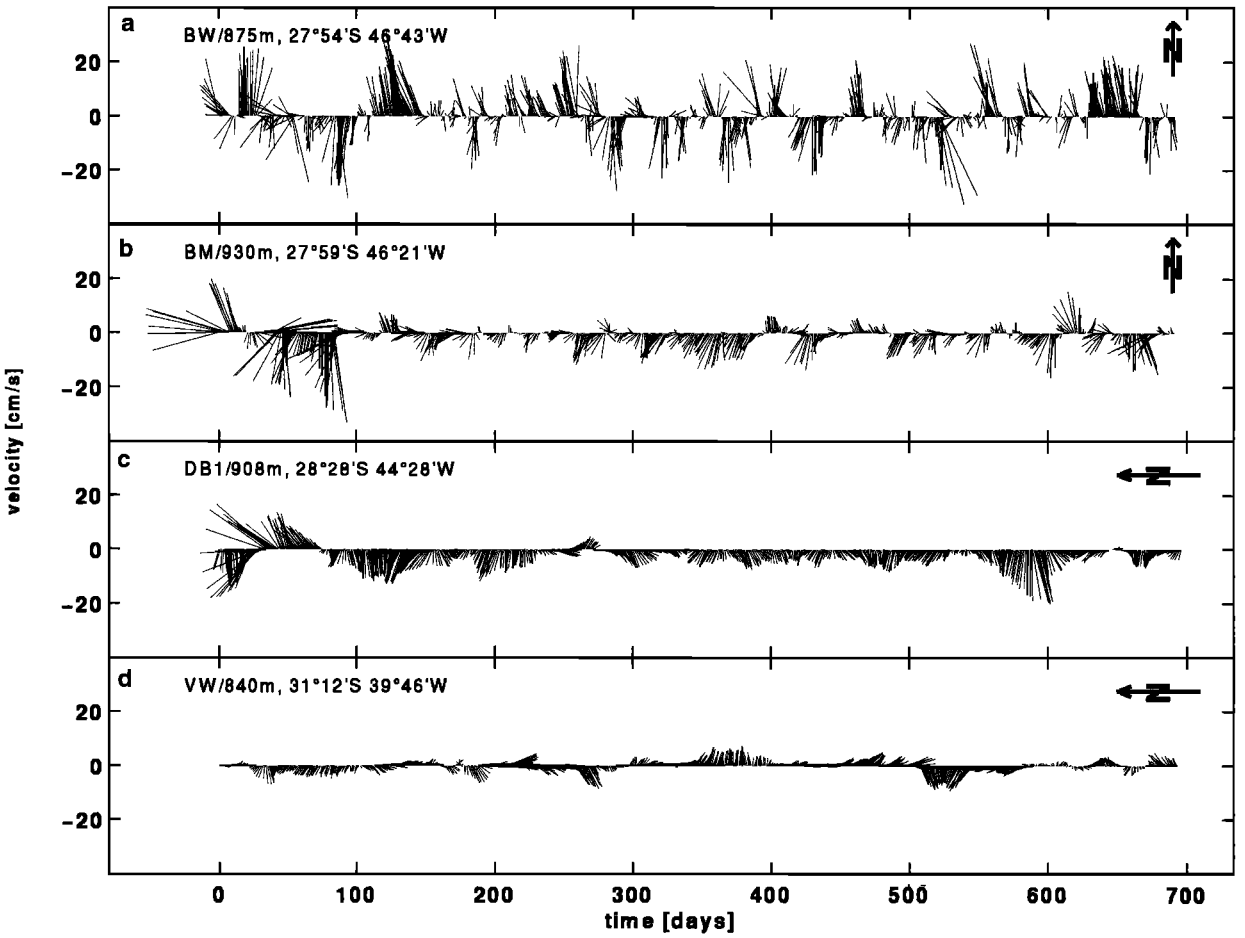

Figure 10. Vector plots from selected current meters. For position, see Figure 2. Note the rotation of the directional frame as indicated by the reference arrow.

current meter records. These are well suited to capture the long-term stability of the velocity field described above because of their record length of nearly 2 years. The mean velocities of the moored instruments are presented in Figure 14 (open arrows) in conjunction with the float box-averaged data. The directions of the mean velocities (Table 2), based on record lengths ranging from 17 to 23 months (except DB2 with a 3 month record length), agree well with the float data.

The errors of the mean velocities presented in Table 2 were estimated according to the method described by *Müller* [1987].

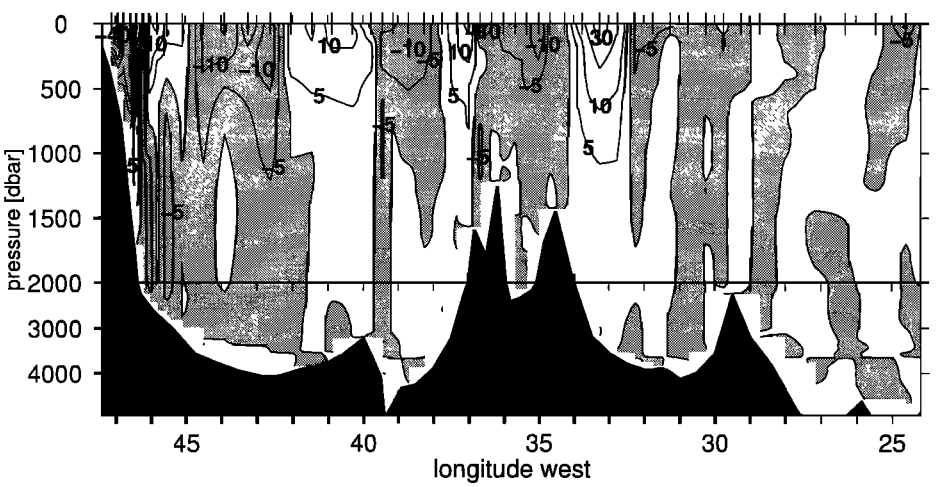

Figure 11. Geostrophic velocity for the 30°S section of Figure 3. Lighter shaded areas indicate southward transport. Note the break of the depth scale at 2000 dbar. Velocity contour lines are spaced 10 cm s^{-1} for $|v| > 10$ cm s^{-1} and 5 cm s^{-1} for $|v| < 30$ cm s^{-1}.

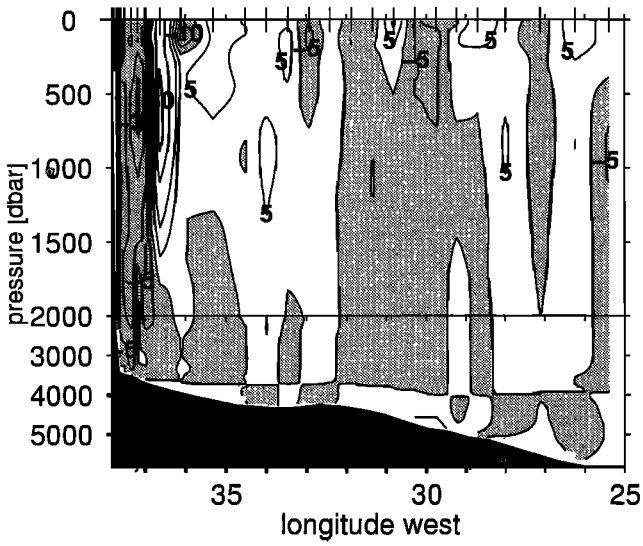

Figure 12. Geostrophic velocity for the 19°S section of Figure 4. Lighter shaded areas indicate southward transport. Note the break of the depth scale at 2000 dbar. Velocity contour lines are spaced 10 cm s^{-1} for $|v| > 30$ cm s^{-1} and 5 cm s^{-1} for $|v| < 10$ cm s^{-1}.

For each instrument, integral timescales (T_{uu} and T_{vv}) were calculated separately for the zonal and meridional components from the integrated autocorrelation function at time lag 100. The calculated timescales are distributed around a mean of T = 16 days and are rather isotropic, except for the two westernmost records, which give T_{uu} = 4 days for the zonal and T_{vv} = 8 days for the meridional and component. On the basis of the mean timescale of T = 16 days the 63% probability error ellipses were calculated according to *Ollitrault* [1994]. Together with the corresponding float box data, these ellipses are presented in Figure 14. The long data records of the order of 2 years reduce the size of these error ellipses, except for current meter DB2, with respect to the corresponding float data error ellipses and, at the same time, confirm the validity of the depicted current field.

The total kinetic energy density corresponding to the sum of the mean and eddy kinetic energy densities (Figure 15 and *Tarbell et al.* [1994]) observed by current meters is of the same order as the box-averaged kinetic energy observed by the floats. Both methods result in energies around 1–2 J m^{-3}, with increasing values closer to the shelf. For the Eulerian data the ratio mke/eke is shifted favoring the eddy kinetic energy, which reflects the influence of the longer records of the current meters. The observed eddy kinetic energies are at the low end of the range of values observed in other regions (e.g., eke > 5 J m^{-3} at 700 dbar in the eastern North Atlantic [*Ollitrault*, 1994]).

The fluctuating data of the westernmost current meter BW (Figure 10) are worth a closer look. The size of the undulating AAIW jet may be determined using data from BW and from the neighboring mooring BM. Figure 16 depicts a three-dimensional (3-D) plot of the normalized, directional displacement from these current meters' records. In each compass plot

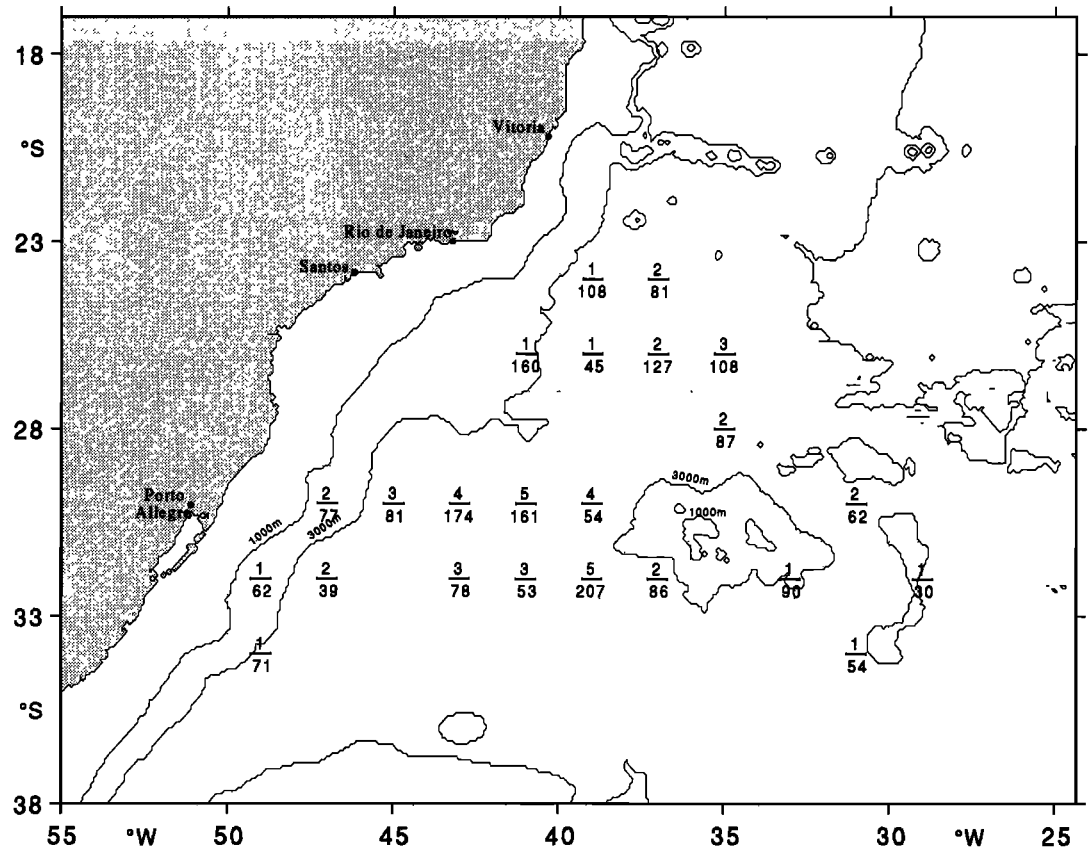

Figure 13. Data density for 2° by 2° boxes. The bottom number gives the number of float days; the top number gives the total number of floats ever occupying that box. The minimum float days per box was set to 30 days, rejecting of the order of 10 boxes which were occupied for shorter periods.

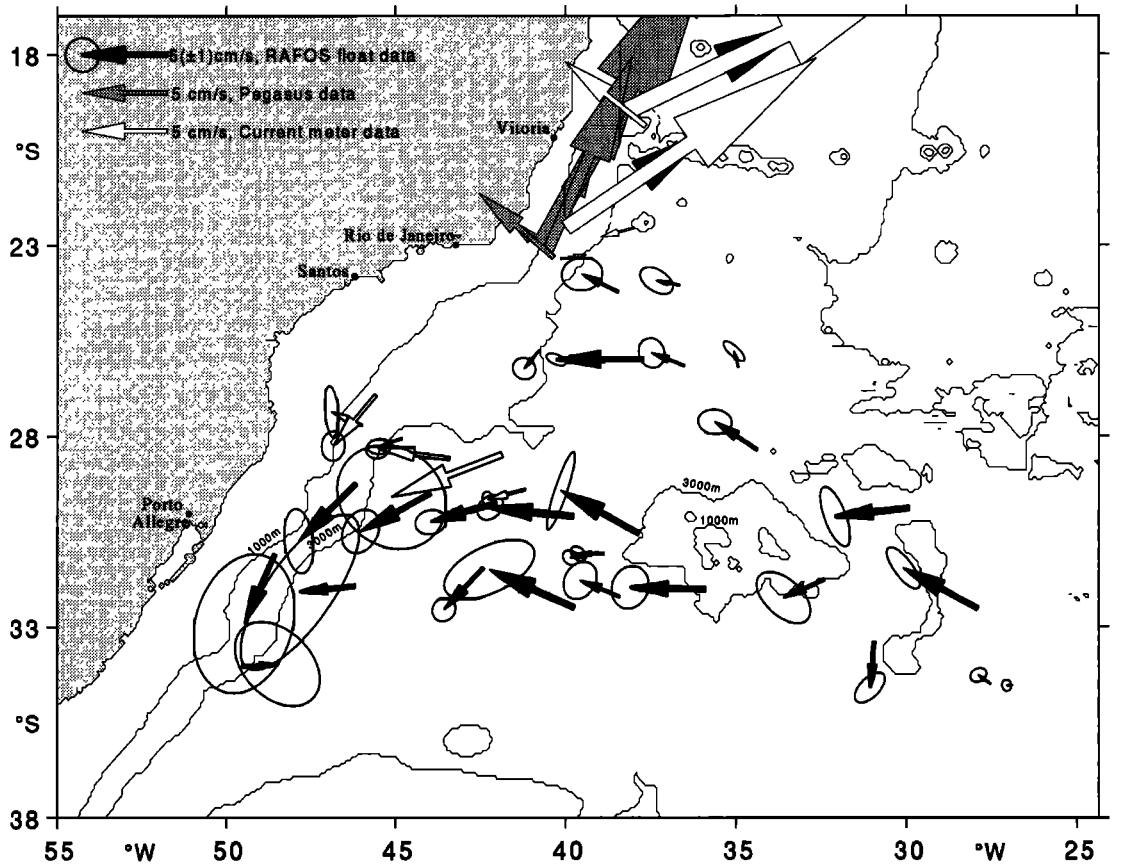

Figure 14. Averages of float velocity (solid arrows) together with current meter data (open arrows) at AAIW depth for 2° by 2° boxes. Additional current meter data were kindly provided by Müller et al. (submitted manuscript, 1996) and J. Lima (personal communication, 1992). Pegasus data [*Garfield*, 1990] at AAIW depth are indicated by shaded arrows. Compare Figure 2 for identification. Probability error ellipses (63%) of float and current meter data around the respective mean velocity vector are included.

the recorded integrated velocity is plotted versus its direction and subsequently normalized to 1 for the maximum value. The normalization factors used are given in Table 4. Clearly, the directional alternation is confined to the AAIW level at the western boundary (BW, 875 m). Above (BW, 670 and 460 m) and to the east of it (BM, all depths) the current flows persistently in south-southwestern directions. This suggests that about 50% of the time, BW captured an isolated northward jet at the AAIW depth dynamically detached from the surrounding water. For the remaining periods the flow is with the surrounding water to the southwest.

From Figure 16 the transport within the western boundary jet close to its creation site can be estimated. The bottom current meter is moored 305 m above the seafloor (1180 m). An upper limit of the jet thickness is given by the position of the current meter above 670 m, which shows little northward transport. This suggests a total jet thickness of $(305 + \frac{1}{2}(875 - 670))$ m $\approx$ 400 m, assuming that the jet is fully developed between the bottom and middepth between the two current meters and negligible above this depth. An estimate for the width of this feature is given similarly by the distance (21 km) to the neighboring mooring BM to the west which shows little transport to the north. Therefore a jet width of half this distance (10 km) was assumed, using a rectangular jet profile of uniform velocity. Thus the transport in the dominant directions 347 and 191°T is roughly estimated to 0.4 and 0.3 Sv on the basis of the velocities given above resulting in an effective northward transport of ~0.1 Sv within this jet, which, however, as noted above, is not significantly different from zero.

In comparison, transports based on the dynamical method are presented in Table 5 and displayed in Figure 17. The evaluation of the hydrographic sections shown in Figures 3 and 4 gives a total northward transport of AAIW in the boundary region north of 26°S. It increases from 1.2 Sv at 26°S to 8.8 Sv at 19°S. The latter result assumes that the two velocity cores observed in this section belong to an eddy (compare Figure 11). The broad band carrying 14.3 Sv of northward transport at 19°S is partly balanced by 6.5 Sv to the south, west of 36.8°W, with a small northward transport making up the 1 Sv difference. South of 27°S, transports near the western boundary are directed poleward with 0.8 Sv at 27°S and between 5.5 and 10.5 Sv around 30°S.

The inflow of water from the east into this area between 23°S and 33°S may be estimated from the float data. A calculation of zonally averaged transports (Figure 18) is performed assuming mean zonal velocities with negligible vertical shear. A mean layer thickness of 500 m is assumed (compare section 3), and the zonally averaged mean box velocities are used. Dashed lines indicate an estimate of the error based on the standard deviation of the zonal average. This calculation yields a total westward transport of AAIW of 15 Sv between 33°S and 23°S. This is close to the sum of geostrophically calculated transports

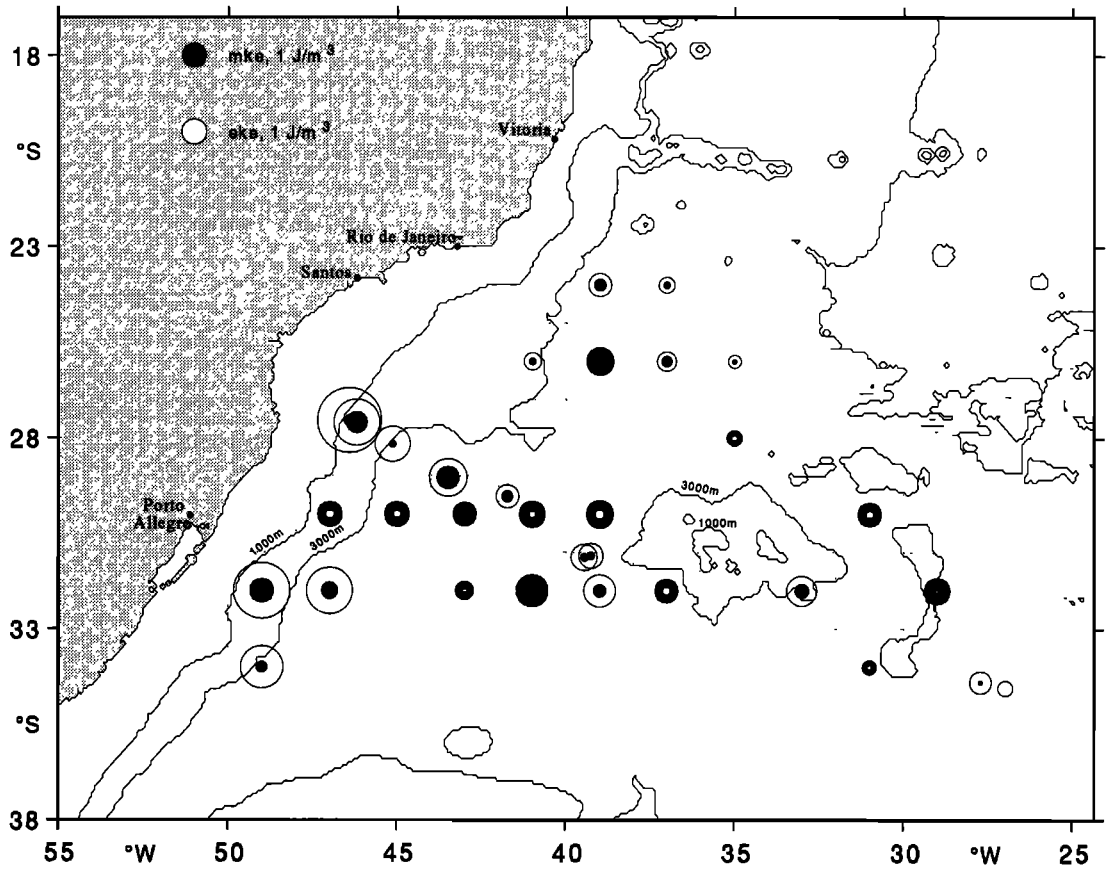

Figure 15. Mean kinetic energy density (mke, solid circles) and eddy kinetic energy density (eke, open circles) for the float data on a 2° by 2° grid and at the respective position for each current meter record (see Figure 2 for the positions of the latter). The area of each circle is proportional to the energy density.

of 8.8 Sv leaving to the north across 19°S and an average of 7.6 Sv flowing south across 30°S along the western boundary.

5. Discussion

The pending question of the AAIW's equatorward pathways is of major importance. As noted in the introduction, three routes (Figure 19) have been suggested in the past: a spreading of fresh AAIW all along the continental slope, the northward flow of AAIW underneath the Brazil Return Current, and the roundabout route following the wind-driven anticyclonic subtropical gyre. The following discussion shall examine these possibilities following the potential routes of AAIW through the South Atlantic using results from our own observations and from the current literature. The section is closed by a comparison of the transports calculated here and those given in the literature.

It is beyond the scope of this study to deal with the formation process of AAIW. Nevertheless, it seems appropriate to start our discussion in the region where the AAIW is formed. A substantial portion of AAIW is likely to be derived from the coldest variety of Subantarctic Mode Water (SAMW) [*England et al.*, 1993; *McCartney*, 1977] formed off southern Chile. This SAMW, also termed Malvinas Water [*Gordon*, 1981], freshens while flowing north to about 40°S–43°S together with the overlying Falkland Current parallel to the western boundary [*Piola and Gordon*, 1989]. At the Brazil-Falkland Confluence Zone it encounters recirculated AAIW from the north [*Peterson and Whitworth*, 1989] with salinities between 34.30 and 34.35. *Maamaatuaiahutapu et al.* [1992] found higher concentrations of AAIW in the north than in the south of their area of study (Figure 2), which emphasizes the influence of recirculated AAIW in the formation process of AAIW. The mixing of recirculated AAIW (Figure 19, label 1) with fresher Malvinas Water from the south generates AAIW with salinities between 34.20 and 34.25 [*Gordon*, 1981], which shall be considered in the following as the primary type of AAIW in the South Atlantic. Our RAFOS data support this concept in that a broad southwestern flow of AAIW is observed between 43°W and 50°W at 30°S (Figure 14).

Once the primary AAIW is formed, it detaches from the western boundary and flows east (Figure 19, label 2) with the South Atlantic Current [*McCartney*, 1977]. This concept was supported recently by Autonomous Lagrangian Circulation Explorer (ALACE) float observations [*Davis et al.*, 1996]. Two instruments deployed in the Drake Passage north of the Polar Front found themselves in the confluence zone in the course of their subsurface drift. Subsequently, they drifted east underneath the South Atlantic Current toward the Mid-Atlantic Ridge showing considerable mesoscale activity.

The eastward flow then meets the Agulhas Water (Figure 19, label 3), forming the source of the recirculating westward flowing AAIW. The collision of the primary AAIW (S = 34.20–34.25) with AAIW from the Indian Ocean (S = 34.50) generates a brand of AAIW characterized by salinities

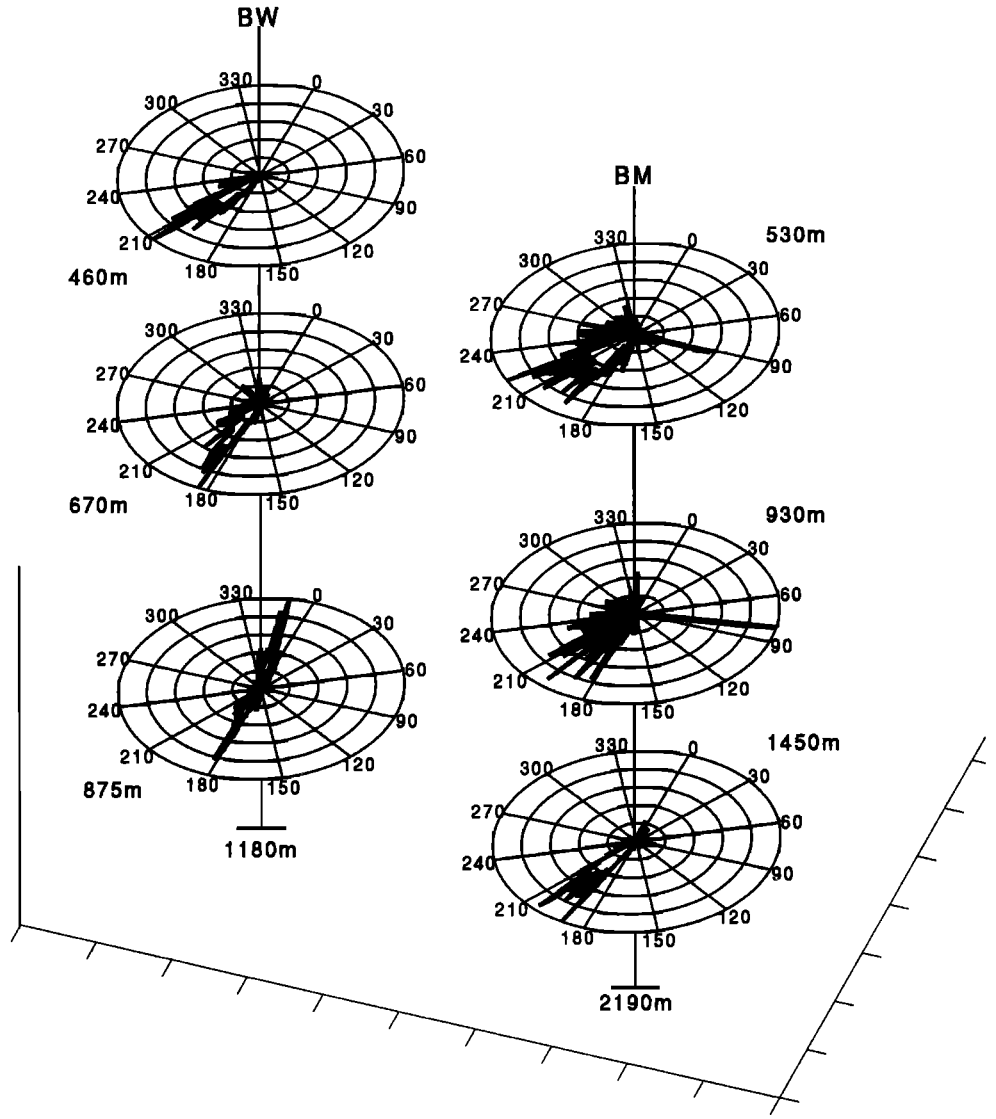

Figure 16. Normalized integrated velocity distribution of current meters of moorings BW and BM around and at the depth level of the AAIW. See Table 4 for normalization factors.

around 34.35–34.38 at the Agulhas Retroflection Zone if admixtures of 50% are assumed [*Gordon et al.*, 1992]. It is water of exactly this salinity range which is found in the area of the presumed northern return flow [*Olbers et al.*, 1992]. A similar scenario is described by *England and Garçon* [1994]. In their model results they observed the formation of the westward flowing northern branch (what they call the Benguela Current) with 25 Sv. It represents the sum of 19 Sv from the South Atlantic Current and 6 Sv of Indian Ocean water. Such a $\frac{3}{4}$ to $\frac{1}{4}$ admixture of primary and Indic AAIW would result in salinities of 34.28–34.31 which are still within the observed range.

Table 4. Relative Normalization Factors used in Figure 16

Mooring	Depth	Factor
BW	460 m	4.8
	670 m	2.1
	875 m	2.1
BM	530 m	1.4
	930 m	1
	1540 m	1.4

The retroflected AAIW is then thought to flow back west, crossing the Mid-Atlantic Ridge. Farther west it is documented in the steady and uniform westward RAFOS float motion of nearly 3 cm s^{-1} (Figure 19, label 4). Marvor floats [*Ollitrault et al.*, 1995] deployed south of the Vitória-Trindade Ridge 1 year after our RAFOS floats also show a continuous westward advection in the open ocean. This indicates a persistent mean flow between 22°S and 32°S offshore beyond the 3000 m isobath. The westward motion of AAIW at the Rio Grande Rise is also confirmed by the results from the current meters at the AAIW level east of 45°W.

Within this westward flow, low-salinity patches (Figure 6) exist within the AAIW layer, which may be explained by their advection and mixing history. A similar variability was already observed by *Reid et al.* [1977], who state that in the southern part of the *Atlantis* 247 section a strong mesoscale activity is evident, indicating several eddies or meanders. In their study, as well as in a comparison of our 30°S and the 19°S sections,

Table 5. Geostrophic Transport Estimates of Antarctic Intermediate Water

Latitude	*Meteor* Cruise	Observation Date	Transport		Boundary Location
			Western Boundary, Sv	Interior, Sv	
19°S	15, leg 3	Feb. 1991	8.8	−0.5	32.0°W
21°S	15, legs 1 and 2	Feb. 1991	4.8	−1.2	39.2°W
24°S	15, legs 1 and 2	Jan. 1991	2.9	...	...
26°S	22, leg 3	Nov. 1992	1.2	...	...
27°S	22, leg 3	Nov. 1992	−0.8	...	...
≈30°S	15, legs 1 and 2	Jan. 1991	−5.5	2.4	39.3°W
≈30°S	22, legs 3 and 4	Nov. 1992	−10.7	3.2	41.0°W
≈30°S	22, leg 5	Dec. 1992	−6.7	6.1	42.0°W

the northern section shows less zonal variability than the southern one. Several causes for the variable salinity in the 30°S section are possible: (1) meanders of, or eddies within, a quasi-zonal westward current of AAIW, (2) local recirculation cells or eddies of southern origin within the large-scale circulation (short circuits), (3) temporal modulations of the primary AAIW constituents at the formation site of this water mass, or (4) temporal variations due to varying mixing at the Agulhas Retroflection Zone.

Considering the first possibility, we ask for the size of the meanders or eddies. The mean amplitude of the salinity fluctuations observed can be inferred from Figure 6 as 0.05 peak to peak. Transposing this estimate into a meridional amplitude using *Reid*'s [1989] map of salinity distribution, this corresponds roughly to a latitudinal excursion of 5° or 500 km. Combined with a zonal interpatch distance of ~1170 km, this would suggest rather large-scale undulations which appear unlikely in view of the steadiness of the float trajectories.

The second possible explanation, the shortcutting of water filaments or eddies of southern origin through an intermediate zone in the gyre center (Figure 19, label 5) cannot be entirely excluded by the existing data. However, if this scenario holds

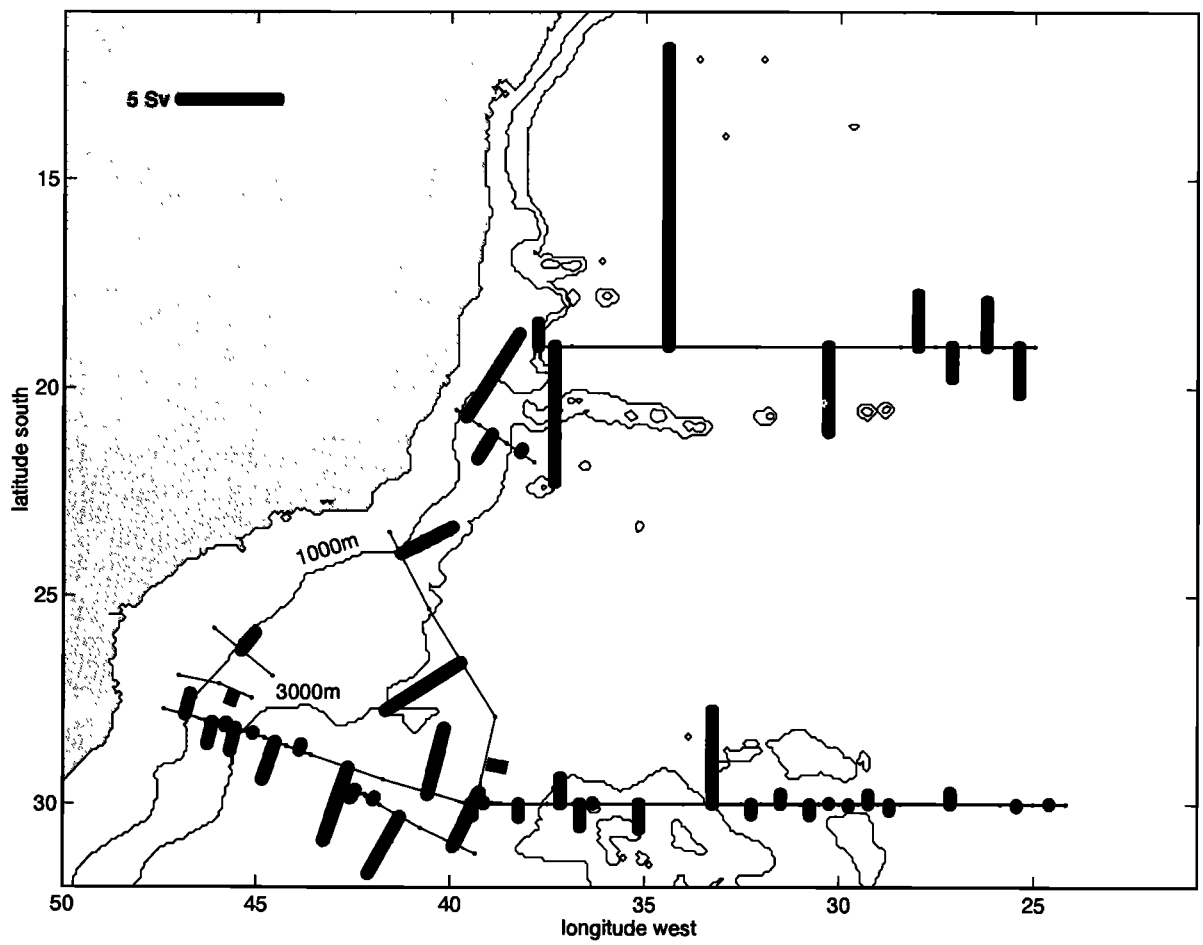

Figure 17. Geostrophic transport of AAIW at the 19°S and 30°S sections as well as for several additional short sections across the Brazil Current. Transports of identical sign for each station pair are accumulated and represented by one bin only.

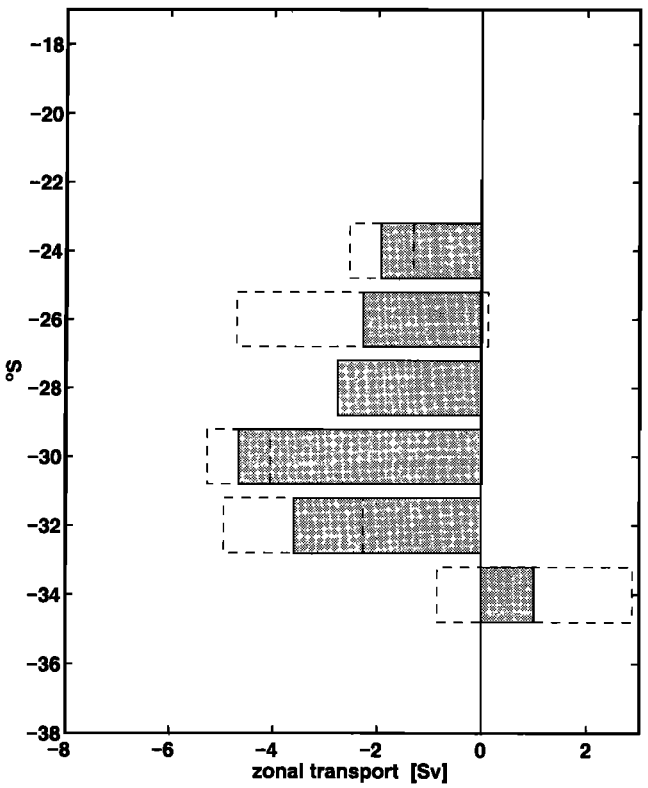

Figure 18. Zonal transports calculated from box-averaged float data. The layer depth was assumed to be 500 m. The dashed lines indicate the transports' standard deviations resulting from the interbox variability of the float velocity box means.

true, much lower salinities should be observed at the 30°S section, resembling more closely the TS properties of their southern origin. So far the central area between 38°S and 34°S has been unvisited by RAFOS or ALACE floats. Covering a long zonal section, the ALACEs [*Davis et al.*, 1996] did not travel north into this intermittent regime. In fact, the instruments stayed south of 38°S during their drift across the Argentine Basin. In addition, our two southernmost current meters at 900 dbar (H3 and H6) deployed southeast of the Rio Grande Rise and actually within this presumed stagnant area show considerably lower means than their counterparts to the northwest (Figure 14 and Table 2). With regard to the 95% error estimates (0.7 and 0.4 cm s^{-1}) their means (0.9 cm s^{-1} at 307 °T and 0.3 cm s^{-1} at 92 °T) are not significantly different from zero, indicating also a zone of stagnation that separates the eastward and westward flowing branches of the gyre. In spite of the low data density the sum of these observations leads to the conclusion that a substantial advective (nondiffusive) exchange between the southern eastward flowing and the northern westward flowing branch is unlikely.

Seasonal variability of the composition of primary AAIW in the confluence region underneath the subtropical thermocline was reported by *Piola and Gordon* [1989] and recently by *Maamaatuaiahutapu et al.* [1992]. They observed distinct differences in source water composition between spring 1989 and winter 1989, with higher concentrations of AAIW in the north and a lower concentration of AAIW in the south during wintertime, i.e., an increased gradient of AAIW concentration during winter. The latter result could be an indication of a seasonal salinity modulation of the primary AAIW. For this signal to be visible in our 30°S section it must be advected all around the gyre, which amounts to roughly 3 years for each leg, assuming a mean zonal velocity of 5 cm s^{-1}. The persistence of seasonal salinity modulations of the order of 0.05 for a number of years, however, seems unlikely in the presence of diffusion if the salinity variation of primary AAIW is assumed to be of the same order [*Piola and Gordon*, 1989].

The assumption of a temporal variation in the Agulhas Retroflection Zone gives a rather simple and likely concept of the low-salinity patches' origin. Surprisingly, these patches are, at least west of 30°W, arranged in a rather regular pattern with an interpatch distance of ~1170 km. In light of an anticyclonic motion of AAIW underneath the subtropical gyre a westward

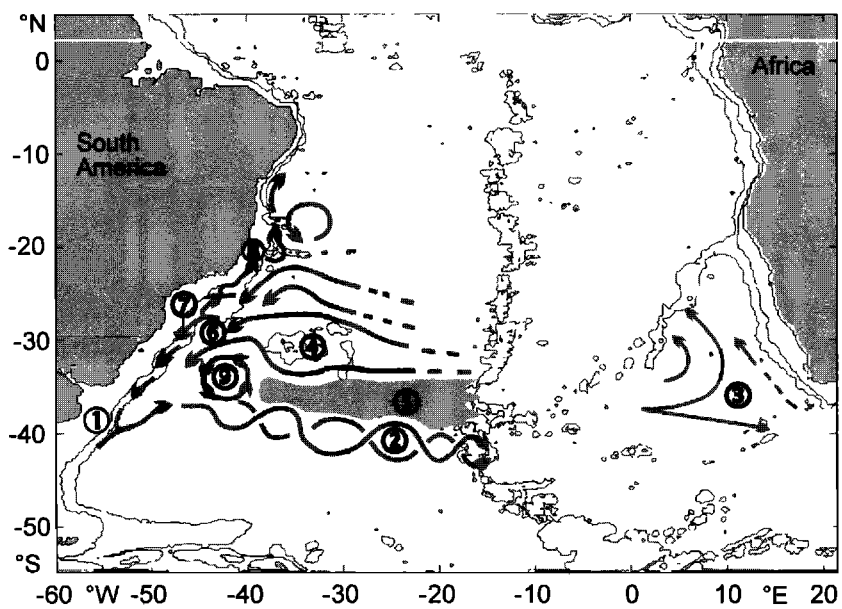

Figure 19. Schematic diagram of the possible pathways of AAIW in the subtropical South Atlantic. The arrows in the east off Africa are according to *Garzoli and Gordon* [1996].

motion of these patches at 30°S is expected. Assuming a seasonal signal in the AAIW concentration, the interpatch distance corresponds to an advection speed of ~4 cm s^{-1} (1170 km yr^{-1} = 3.7 cm s^{-1}). This result agrees well with the mean westward float velocity; however, it might be fortuitous. The fact that the amplitude of the salinity variation ΔS of these patches is stronger in the east than in the west points toward their eastern origin, whereas the westward increasing size points to the effect of ongoing diffusion.

When the westward flow approaches the South American shelf, the floats exhibit a deflection to the south in the vicinity of the 3000 m isobath (Figure 19, label 6). A northward advection along the western boundary was not observed by these floats. Evidence for a divergence (Figure 19, label 7) of the westward flow, however, is found in the current meter record at 875 m depth at the shelf break (BW). This mooring (Table 2) appears to have been placed right at the site of bifurcation, recording the bimodal current structure already presented in Figures 10 and 16. The position of this divergence site is confirmed by Marvor float data [*Ollitrault et al.*, 1995] depicting the northward deflection of floats intruding into the waters above the Santos Plateau at approximately 28°S. These results support the idea that it is recirculated and blended AAIW from the eastern South Atlantic that contributes the bulk if not all of the water to the northward shelf-trapped jet of AAIW. The deflection of the AAIW to the southwest is confirmed by the results from current meters at the AAIW level moored at the southern perimeter of the Santos Plateau as well as from the float trajectories of both RAFOS and Marvor floats.

The existence of a northward flow along the shelf (Figure 19, label 8) north of 25°S and its extension into the northern Brazil Basin is bolstered by many studies. Pegasus velocity profile measurements were performed by *Evans and Signorini* [1985] and later reanalyzed by *Garfield* [1990]. They observed a northeastward flow of AAIW at 20°30′S (occupied once) in the Vitória-Trindade Ridge and between 23°S and 24°S (occupied three times) with velocities between 10 and 35 cm s^{-1} at a depth of ~800 m, suggesting a northward flowing jet of AAIW at the shelf break of <20 km width and ~400 m vertical extension. The maximum velocities found at the shelf were larger than 30 cm s^{-1} in April 1983 and around 20 cm s^{-1} in October 1983. To the south, only one Pegasus profile exists at 31°S, indicating a much smaller velocity of about 5 cm s^{-1} to the northwest at 700 m [*Garfield*, 1990, Figure 3.3c]. Data from northern current meters (M1, M2, L1, and L2 in Figures 2 and 14) indicate a persistent northward transport along the 1000 m isobath north of 23°S. Strong northward currents were observed by M1 and L1, suggesting the inflow of AAIW into the northern Brazil Basin through channels in the Vitória-Trindade Ridge (T. J. Müller et al., Direct measurements of western boundary currents off Brazil between 19°S and 28°S, submitted to *Journal of Geophysical Research*, 1996) (hereinafter referred to as Müller et al., submitted manuscript, 1996). This inflow seems to be confined to a narrow shelf-trapped jet, since the current meters farther offshore (M2 and L2) show considerably smaller means. Recently, such a flow pattern was also confirmed by results from Marvor floats, which followed a northward course at the shelf and actually crossed the Vitória-Trindade Ridge from south to north [*Ollitrault et al.*, 1995].

Finally, the question remains if a direct, shelf-trapped, northward path of AAIW exists at latitudes between 40°S and 28°S. A tongue of low-salinity water being interpreted in such a way is observed along the western boundary on isopycnal surfaces by *Zemba* [1991] and *Suga and Talley* [1995]. However, it is neither visible in the new sections presented here nor in maps presented on isopycnal surfaces σ_0 = 27.18 kg m^{-3} [*Reid et al.*, 1977] and σ_0 = 27.30 kg m^{-3} [*Reid*, 1989]. Interestingly, *Tsuchiya et al.* [1994] depict a salinity tongue juxtaposed to that of Suga and Talley using the same cruise data as both Zemba and Suga and Talley, however, representing salinity on a slightly shallower isopycnal surface σ_0 = 27.2 kg m^{-3}. This suggests an alternative interpretation, favoring small-scale fluctuation in the salinity distribution, rather than a permanent long-range feature with oceanographic implications. As discussed above, our sections spanning the Brazil Current (Figure 5) show a distinct salinity minimum only in the northern part, suggesting that no continuous northward current exists. A bifurcation of the westward return flow at 28°S, however, can easily explain a northern tongue, whereas no such tongue should appear in the south.

The absence of a direct northward flow at these latitudes is further supported in a tracer study by *Warner and Weiss* [1992]. Reproducing the northward salinity tongue along the South American coast north of 20°S, they find a CFC concentration in this area which excludes the direct connection of the former to the newly ventilated waters of the confluence zone. In summary, the hydrographic sections presented in section 3 and a modified interpretation of recent publications suggest the absence of a persistent northward extending low-salinity tongue between the confluence zone and 28°S.

Primarily on the basis of the floats' northward excursion at the Vema Channel, a permanent offshore northward transport of AAIW, as suggested by *Zemba* [1991], cannot entirely be excluded. Judging from the trajectories (Figure 7), however, it is probably a local loop (Figure 19, label 9), possibly causing mixing of the westward return flow water with fresher water from the south through entrainment, rather than a continuous flow across 30°S to the north. It is noted that the northward excursion at 31°S, 40°W is also shown by *Reid et al.*'s [1977, Figure 9] map of geopotential anomaly.

The presented concept shall finally be reviewed with regard to the transports ascribed to the individual branches of the flow. In the west the AAIW formation region is characterized by the inflow of a 7.6 Sv (Table 5, average of western boundary transport at 30°S) of recirculating AAIW from the north which is smaller than the 17 Sv calculated by *England and Garçon* [1994]. However, their definition of Intermediate Water (IW) (above 1500 dbar and colder than 9°C) results in a layer thickness of about 800 m at 30°S, explaining the more than doubled values. This southwestward transport is derived from a westward transport of the order of 15 Sv (Figure 18) north of 33°S, within the northern branch of the gyre. This is considerably smaller than the 25 Sv of IW presented by *England and Garçon* [1994], but again, the discrepancy is explained by the difference in the assumed layer thickness.

The calculated northward transport at the western continental shelf is of the order of 0.4 Sv at 28°S and much lower than the 3.5 Sv at 24°S (Figure 2) between 400 and 1300 m as given by *Garfield* [1990] or the 5 Sv observed by *Fu* [1981]. The estimated vertical limits of the jet at 28°S (400 m height by 10 km width) are increasing twofold in both lateral directions at 24°S [*Garfield*, 1990, Figures 3.5a and 3.5b]. The velocity picks up by a factor of 2 and thus accounts for the 3.5 Sv observed in the later study, also assuming that the jet has stabilized in time. Thus this Intermediate Western Boundary Current should be pictured as a very narrow jet, taking off from 28°S and farther

north and increasing steadily in size and velocity (compare Table 5, western boundary transport between 19°S and 26°S). It is confined toward the interior by the southward flowing, recirculated AAIW, and its actual source wanders north and south around 28°S with time. *England and Garçon* [1994] find a transport of 8 Sv to the north, which agrees nicely with the 9 Sv found at 19°S (Table 5) in this study. However, this number also comprises a contribution outside the western boundary regime. This northward transport would adequately contribute to the compensation of 15 to 20 Sv of southward NADW flow [*Gordon*, 1986] if *Rintoul*'s [1991] findings of a nearly equal split between thermocline water (8 Sv), AAIW (5 Sv), and bottom water (4 Sv) crossing 32°S are accepted.

Acknowledgments. The experimental phase of our studies was supported by the Deutsche Forschungsgemeinschaft (contracts Si 111/39-1 and Ze 145/6-1). The help of Captain G. Müller and his *Meteor* crew is well recognized. We benefited from unpublished current meter records provided by our colleagues T. J. Müller (IfM Kiel) and J. Lima (Petro-Bras, Rio de Janeiro). Not forgotten is the excellent cooperation of Y. Ikeda, University of São Paulo. The analytical phase of our work is funded by the Ministerium für Bildung, Wissenschaft, Forschung und Technologie under contract FK 03F0121A as a contribution to the World Ocean Circulation Experiment (WOCE).

References

Boebel, O., K. Schultz Tokos, and W. Zenk, Calculation of salinity from neutrally buoyant RAFOS floats, *J. Atmos. Oceanic Technol.*, *12*(4), 923–934, 1995.

Broecker, W. S., D. Peteet, and D. Rind, Does the ocean-atmosphere have more than one stable mode of operation?, *Nature*, *315*, 21–25, 1985.

Buscaglia, J. L., On the circulation of the Intermediate Water in the southwestern Atlantic Ocean, *J. Mar. Res.*, *29*, 245–255, 1971.

Davis, R. E., P. D. Killworth, and J. R. Blundell, Comparision of Autonomous Lagrangian Circulation Explorer and fine resolution Antarctic model results in the South Atlantic, *J. Geophys. Res.*, *101*(C1), 855–884, 1996.

Deacon, G. E. R., The hydrology of the Southern Ocean, *Discovery Rep.*, *15*, 1–124, 1937.

Defant, A., Quantitative Untersuchungen zur Statik und Dynamik des Atlantischen Ozeans, in *Wiss. Ergebn. Dtsch. Atlant. Exped. "Meteor"*, vol. 6, pp. 191–260, Walter de Gruyter, Berlin, Germany, 1941.

England, M. H., and V. Garçon, South Atlantic Ocean ventilation: A numerical model study with geochemical tracers, *Ann. Geophys.*, *11*, suppl. II, C163, 1993.

England, M. H., and V. C. Garçon, South Atlantic circulation in a world ocean model, *Ann. Geophys.*, *12*, 812–825, 1994.

England, M. H., J. S. Godfrey, A. C. Hirst, and M. Tomczak, The mechanism for Antarctic Intermediate Water renewal in a world ocean model, *J. Phys. Oceanogr.*, *23*, 1553–1560, 1993.

Evans, D. L., and S. R. Signorini, Vertical structure of the Brazil Current, *Nature*, *315*, 48–50, 1985.

Fu, L.-L., The general circulation and meridional heat transport of the subtropical South Atlantic determined by inverse methods, *J. Phys. Oceanogr.*, *11*, 1171–1193, 1981.

Garfield, N., The Brazil Current at subtropical latitudes, Ph.D. thesis, Univ. of R. I., Kingston, 1990.

Garzoli, S. L., and A. L. Gordon, Origins and variability of the Benguela Current, *J. Geophys. Res.*, *101*(C1), 897–906, 1996.

Gordon, A. L., South Atlantic thermocline ventilation, *Deep Sea Res.*, *Part A*, *28*(11), 1239–1264, 1981.

Gordon, A. L., Interocean exchange of thermocline water, *J. Geophys. Res.*, *91*(C4), 5037–5046, 1986.

Gordon, A. L., R. F. Weiss, W. M. Smethie Jr., and M. J. Warner, Thermocline and intermediate water communication between the South Atlantic and Indian Oceans, *J. Geophys. Res.*, *97*(C5), 7223–7240, 1992.

König, H., and W. Zenk, Principles of RAFOS technology at the Institut für Meereskunde Kiel, *Ber. 222*, 99 pp., Inst. für Meereskunde, Kiel, Germany, 1992.

Maamaatuaiahutapu, K., V. C. Garçon, C. Provost, M. Boulahdid, and A. P. Osiroff, Brazil-Malvinas Confluence: Water mass composition, *J. Geophys. Res.*, *97*(C6), 9493–9505, 1992.

Marchesiello, P., Simulation de la circulation océanique dans l'Atlantique Sud avec un modèle numérique à coordonée sigma, Ph.D. thesis, Univ. Joseph Fourier, Grenoble, France, 1995.

McCartney, M. S., Subantarctic Mode Water, in *A Voyage of Discovery, George Deacon Anniversary Volume*, edited by M. Angel, pp. 103–119, Pergamon, Tarrytown, N. Y., 1977.

Müller, T. J., Analyse niederfrequenter Stromungsschwankungen im Nordostatlantik, *Ber. 170*, 134 pp., Inst. für Meereskunde, Kiel, Germany, 1987.

Muller, T. J., N. Zangenberg, Y. Ikeda, P. Leao, and W. H. Pinaya, Direct measurement of western boundary currents off the Brazilian coast, paper presented at Symposium: The South Atlantic: Present and Past Circulation, Fachbereich Geowiss., Univ. Bremen, Bremen, Germany, Aug. 15–19, 1994, 1994.

Olbers, D., V. Gouretski, G. Seiss, and J. Schröter, *Hydrographic Atlas of the Southern Ocean*, 82 pp., Alfred Wegener Inst., Bremerhaven, Germany, 1992.

Ollitrault, M., The Topogolf Experiment: Lagrangian data, technical report, Inst. Fr. de Rech. pour l'Exploit. de la Mer, Cent. de Brest, Brest, France, 1994.

Ollitrault, M., Y. Auffret, N. Cortès, C. Hémon, P. Jégou, S. Le Reste, G. Loaec, and J.-P. Rannou, The SAMBA experiment: SAMBA I Lagrangian and CTD data, February 1994–August 1995, technical report, Inst. Fr. de Rech. pour l'Exploit. de la Mer, Plouzané, France, 1995.

Peterson, R. G., The boundary currents in the western Argentine Basin, *Deep Sea Res.*, *Part A*, *39*(3/4), 623–644, 1992.

Peterson, R. G., and T. Whitworth III, The subantarctic and polar fronts in relation to deep water masses through the southwestern Atlantic, *J. Geophys. Res.*, *94*(C8), 10,817–10,838, 1989.

Piola, A. R., and A. L. Gordon, Intermediate waters in the southwest South Atlantic, *Deep Sea Res.*, *Part A*, *36*(1), 1–16, 1989.

Reid, J. L., On the total geostrophic circulation of the South Atlantic Ocean: Flow patterns, tracers, and transports, *Prog. Oceanogr.*, *23*(3), 149–244, 1989.

Reid, J. L., W. D. Nowlin, and W. C. Patzert, On the characteristics and circulation of the southwestern Atlantic Ocean, *J. Phys. Oceanogr.*, *7*, 62–91, 1977.

Richardson, P. L., SOFAR floats give a new view of ocean eddies, *Oceanus*, *34*, 23–31, 1991.

Rintoul, S. R., South Atlantic interbasin exchange, *J. Geophys. Res.*, *96*(C2), 2675–2692, 1991.

Rossby, T., Five drifters in a Mediterranean salt lens, *Deep Sea Res.*, *Part A*, *35*(9), 1653–1663, 1988.

Schmid, C., H. Schäfer, G. Podestá, and W. Zenk, The Vitória Eddy and its relation to the Brazil Current, *J. Phys. Oceanogr.*, *25*, 2532–2546, 1995.

Schmitz, W. J., Jr., On the interbasin-scale thermohaline circulation, *Rev. Geophys.*, *33*(2), 151–173, 1995.

Siedler, G., and W. Zenk, WOCE Sudatlantik 1991, Reise nr. 15, 30. Dezember 1990–23. März 1991, *Meteor Ber. 92-1*, 127 pp. Univ. Hamburg, Hamburg, Germany, 1992.

Siedler, G., W. Balzer, T. J. Müller, R. Onken, M. Rhein, and W. Zenk, WOCE South Atlantic 1992, Cruise no. 22, 22 September 1992–31 January 1993, *Meteor Ber. 93-5*, 131 pp., Univ. Hamburg, Hamburg, Germany, 1993.

Stramma, L., and R. Peterson, The South Atlantic Current, *J. Phys. Oceanogr.*, *20*, 846–859, 1990.

Suga, T., and L. D. Talley, Antarctic Intermediate Water circulation in the tropical and subtropical South Atlantic, *J. Geophys. Res.*, *100*(C7), 13,441–13,453, 1995.

Sverdrup, H. U., M. W. Johnson, and R. H. Fleming, *The Oceans: Their Physics, Chemistry and General Biology*, 1087 pp., Prentice-Hall, Englewood Cliffs, N. J., 1942.

Taft, B. A., Distribution of salinity and dissolved oxygen on surfaces of uniform potential specific volume in the South Atlantic, South Pacific, and Indian Oceans, *J. Mar. Res.*, *21*, 129–146, 1963.

Tarbell, S., R. Meyer, N. Hogg, and W. Zenk, A moored array along the southern boundary of the Brazil Basin for the Deep Basin Experiment—Report on a joint experiment 1991–1992, *Ber. 243*, Inst. für Meereskunde, Kiel, Germany, 1994.

Tsuchiya, M., L. D. Talley, and M. S. McCartney, Water-mass distribution in the western South Atlantic: A section from South Georgia

Island (54S) northward across the equator, *J. Mar. Res.*, *52*, 55–81, 1994.

von Schubert, O., Die Stabilitätsverhältnisse im Atlantischen Ozean, *Wiss. Ergebn. Dtsch. Atlant. Exped. "Meteor,"* vol. 6, 54 pp., Walter de Gruyter, Berlin, Germany, 1935.

Warner, M. J., and R. F. Weiss, Chlorofluoromethanes in the South Atlantic Antarctic Intermediate Water, *Deep Sea Res., Part A*, *39*, 2053–2075, 1992.

World Climate Research Program (WCRP), WOCE implementation plan, World Climate Research Program 11, *Tech. Rep. WMO/ITD 242*, 74 pp., Geneva, Switzerland, 1988.

World Climate Research Program (WCRP), WOCE data handbook: WHP one-time survey standards for water samples, report, World Ocean Circ. Exp. Int. Proj. Off., Wormley, England, 1994.

Wüst, G., Schichtung und Zirkulation des Atlantischen Ozeans, Die Stratophäre, in *Wiss. Ergebn. Dtsch. Atlant. Exped. "Meteor,"* vol. 6, 180 pp., Walter de Gruyter, Berlin, Germany, 1935.

Zemba, J. C., The structure and transport of the Brazil Current between 27° and 36° South, Ph.D. thesis, Mass. Inst. of Technol./Woods Hole Oceanogr. Inst., Cambridge, 1991.

Zenk, W., and T. J. Müller, WOCE Studies in the South Atlantic: Cruise no. 28. 29 March 1994–14 June 1994, *Meteor Ber. 95-1*, 193 pp., Univ. Hamburg, Hamburg, Germany, 1995.

O. Boebel, Department of Oceanography, University of Cape Town, Private Bag, Rondebosch, 7701 South Africa. (e-mail: oboebel@physci.uct.ac.za)

C. Schmid and W. Zenk, Institut für Meereskunde, Universität Kiel, Düsternbrooker Weg 20, 24105 Kiel, Germany.

(Received March 22, 1996; revised December 13, 1996; accepted January 29, 1997.)